RICE UNIVERSITY

Geochemical Diagnostics of Metasedimentary Dark Inclusions: a Case Study from the Peninsular Ranges Batholith, California

by

Kelley Z. Liao

A THESIS SUBMITTED
IN PARTIAL FULFILLMENT OF THE
REQUIREMENTS FOR THE DEGREE

Master of Science

APPROVED, THESIS COMMITTEE:

Cin-Ty Lee
Professor Earth Science

Rajdeep Dasgupta
Professor Earth Science

Adrian Lenardic
Professor Earth Science

HOUSTON, TEXAS
AUGUST 2012

Acknowledgements

First and foremost, I would like to thank my advisor Cin-Ty Lee for his patience, guidance, advice, and knowledge throughout these years. I have learned crucial lessons not only about science and research but also about ownership of everything that one accomplishes or does not accomplish in life. I would also like to thank my committee members Adrian Lenardic and Rajdeep Dasgupta for their knowledge and insights both in shaping this thesis and in the classroom. Special thanks goes out to Doug Morton for making this project possible and providing his extensive knowledge in the field. My gratitude also extends to my lab mates, Emily Chin, Monica Erdman, Anukriti Sharma, and Peter Luffi, for the unwavering help and encouragement they've given me. The support I've received from friends and family has also been crucial to the completion of my thesis. In particular, I would like to thank Sun Ya, Ayca Agar Cetin, Echo Ding, Chinh Nguyen, and Pranabendu Moitra for their friendship in the department. I also owe special thanks to Mary Ann Lebar for all her help and support in the logistics of meeting departmental and university graduate requirements. Finally, to my family, I owe everything.

Abstract

Geochemical diagnostics of metasedimentary dark inclusions: a case study from the Peninsular Ranges Batholith, California

By

Kelley Z. Liao

Dark enclaves rich in amphibole and biotite are ubiquitous in granitoid rocks and can represent fragments of mafic magmas, cumulates, restites, or country-rock. To develop criteria for identifying dark enclaves of non-magmatic origin, we investigated dark enclaves from a complete spectrum of light (carbonate- or feldspar-rich) to dark (amphibole-rich, biotite-rich, or composite) enclaves, reflecting progressive thermal and chemical equilibration with host tonalite from the Domenigoni Valley pluton in the Peninsular Ranges Batholith, California. Metasedimentary dark enclaves have geochemical characteristics that overlap those of literature-compiled igneous dark enclaves. Comparison to modeled igneous differentiation paths shows metasedimentary enclaves can have anomalous CaO and K_2O contents for a given SiO_2, but other major element systematics may not deviate noticeably from igneous differentiation trends. In addition, the fact that there are literature-compiled mafic enclaves trending towards high K_2O and high CaO suggests that not all mafic enclaves are of igneous origin. This work provides some criteria for identifying enclaves should a case of metasedimentary origin arise.

Table of Contents

List of Figures

List of Tables

1. Introduction

Dark inclusions rich in mafic minerals are ubiquitous in granitoid plutons. (Didier, 1973; Eichelberger, 1975; Frost and Mahood, 1987; Vernon, 1990; Poli and Tommasini, 1991; Blundy and Sparks, 1992; Tobisch, 1997; Wiebe, 1997; Barbarin, 2004). Often referred to as "mafic enclaves", these inclusions have high abundances of minerals such as biotite and amphibole. Dark enclaves are generally thought to represent fragments of entrained cumulates, restites, or mafic magmas and hence interpreted to reflect igneous origins (White and Chappell, 1977; Dodge and Kistler, 1990; Blundy and Sparks, 1992; Chappell, 1995). However in some instances, dark enclaves may reflect fragments of sedimentary and metamorphic country rock that have been entrained in a pluton body (Phillips, 1981; Price, 1983; Chen, 1989; Maas et al., 1997). Following entrainment, these country rock fragments are metamorphosed. Specifically, country rock rich enough in Ca or K and Al can be thermally metamorphosed into amphibole-rich and biotite-rich rocks, respectively. As a result, the dark macroscopic appearance of these non-magmatic enclaves can resemble igneous enclaves (Figure 1). Although it is unclear whether a metasedimentary origin for mafic enclaves is significant compared to igneous origins, erroneously attributing metasedimentary dark enclaves to igneous protoliths will lead to misunderstanding of how magmas are generated, emplaced and differentiated. For example, assimilation of sedimentary country rock may release more volatiles, such as CO_2, H_2O (Dyer, 2011) and various S species, than intrusion of mafic magmas into felsic magmas.

There is thus a need to develop criteria for identifying the protoliths of dark enclaves. Towards these ends, we examine a suite of dark enclaves from a tonalitic pluton in the Cretaceous northern Peninsular Ranges Batholith in southern California (Figure 2). These enclaves have unequivocal metasedimentary protoliths and are present in various stages of

thermal and chemical equilibration with the host magma, resulting in the generation of dark enclaves that appear superficially like typical igneous mafic enclaves. This case study provides an opportunity to develop some criteria for identifying non-magmatic dark enclaves.

2. Geologic Background

The Cretaceous Peninsular Ranges Batholith extends from southern California through Baja California (Figure 2). Three zones within the batholith can be distinguished based on the composition of their prebatholithic rocks (Gastil, 1975; Gromet and Silver, 1987; Todd et al., 1988). Pre-batholithic rocks in the western region consist of late Jurassic and early Cretaceous subaerial and submarine volcanic and volcaniclastic rocks thought to be an accreted island arc. Pre-batholithic rocks in the central portion are Triassic to Cretaceous continental-derived flysch sediments, and in the eastern zone they are passive margin clastic sediments (Wetmore et al., 2003). The Peninsular Ranges Batholith was emplaced through these rocks in the mid- to late Cretaceous (140 and 80 Mya) in an ocean-continent subduction zone setting (Kistler et al., 2003).

Our study region is a pluton-wallrock contact zone in the Domenigoni Valley Pluton, located in the northern Peninsular Ranges Batholith near Sun City in Riverside County, California (Figure 3) (Morton, 1999). The pluton is composed of biotite and hornblende tonalite, and it intruded Triassic phyllites, greywackes, dirty quartzites, carbonate-bearing quartzites and interbedded phyllites with quartzites. Assimilation of these metasediments is evident in roadcuts on the western margin of the pluton. Fragments of metasediments as well as dark enclaves are exposed in roadcuts of the Domenigoni Valley Pluton along the 215 Freeway in Sun City (33° 42’ 8.65” N, 117° 10’ 54.95” W).

3. Methods

Whole rock analysis of major and trace element abundances for the various enclave types were carried out by ICP-AES mass spectrometry and XRF at USGS laboratories. All analyses of individual mineral phases were completed at Rice University using laser ablation inductively coupled plasma mass spectrometry (ICP-MS) on a Thermo Finnigan Element 2 equipped with a 213 nm New Wave laser ablation system. Standard thick sections (200 μm) were analyzed with the laser ICP-MS. External standards used during LA-ICP-MS analysis included BHVO2g, BCR2g, BIR1, and NIST612. Laser ablation was conducted with a fluence of 19 J/cm^2, frequency of 10 Hz, and a spot size of 55 μm. Under these conditions, instrument sensitivity was 120,000 cps on 15 ppm La in low mass resolution (m/Δm~300). Raw data from LA-ICP-MS was reduced using a program that removes background signal intensities in each analysis. Then, time-resolved signals for various elements analyzed are selected with the criteria they are parallel, in order to avoid interference from contaminant phases. The remaining signal intensities are normalized to an internal standard. Si^{30} was used as the internal standard for all mineral phases measured in mid resolution, while Mg^{25} was used for biotite and hornblende analysis in low resolution. Normalizing to an internal standard corrects for the fact that ablating samples under varying conditions will affect the absolute signal intensities.

4. Results

4.1 Petrography

4.1.1 Tonalite

The host tonalite is composed of approximately 10% amphibole, 15% biotite, 30% quartz and 40% plagioclase. Accessory phases include zircon, Fe-Ti oxides, and titanite. Texturally, the tonalite is medium-grained to coarse-grained with subhedral to euhedral plagioclase grains surrounded by mostly anhedral quartz, biotite and amphibole. Plagioclases show polysynthetic albite twinning but also show crystallographic radial and sector zoning, the latter typical of magmatic feldspars. Many of the plagioclase cores also have a corroded appearance due to the presence of many micron-scale inclusions of fluids, biotite and amphibole, typical of magmatic crystallization textures (Barbarin, 1990; Hibbard, 1995). Some of the inclusions are carbonates. Quartz displays undulose extinction. Amphibole and biotite are anhedral and often occur as intergrown aggregates. Biotite can also be found as aggregates surrounding large plagioclase crystals. Accessory titanite typically occurs as thin rims (<.05 μm) around Fe-Ti oxide grains.

4.1.2 Enclaves

Enclaves range in size from decimeters to meters and can be classified as dark enclaves abundant in mafic mineral phases and lighter-colored enclaves abundant in quartz and variable amounts of carbonate. Both enclave types are fine-grained. Grains are almost entirely anhedral, with grain boundaries between quartz and feldspars showing well equilibrated textures, e.g., 120° triple junctions.

Dark enclaves

We categorize the dark enclaves based on their dominant mafic mineral phase (Table 1 and Figure 4). The amphibole-rich group is composed of quartz (~60%), amphibole (~30%) and

minor plagioclase. These enclaves exhibit subtle foliation defined by 1-5 mm thick amphibole-rich bands. Clinopyroxene is present in trace amounts and often appears to be replaced by amphibole. At the contact between the amphibole-rich enclave and the host tonalite, there is a <1 mm biotite-rich rim, reflecting K diffusion from tonalite to enclave (cf. Johnston and Wyllie, 1988).

The biotite-rich group is dominated by quartz (~50%) and biotite (~40%) with small amounts of alkali feldspar. Some of the biotite-rich enclaves are finely foliated, reflecting relict metamorphic foliation. Fe-Ti oxide minerals are a common accessory phase and often found in association with biotite grains.

Composite enclaves, containing both of the above lithologies in the form of alternating bands are also present and may indicate macro-scale compositional heterogeneities in the protolith.

Light enclaves

Light enclaves are dominantly composed of quartz, but can be classified into two groups. The first group is composed of carbonate-bearing quartzites, containing 60 to 80% quartz and variable amounts of wollastonite (0-30%), diopside (0-20%), and carbonate (5-15%) (Table 2). These enclaves are fine-grained and consist of anhedral grains showing well-equilibrated granular textures manifested as 120° triple junctions. Quartz grains range from 1-10 μm. Pyroxenes and carbonates are much finer grained, with individual grains no larger than 2 μm. Wollastonite and diopside often appear as bands cutting through the enclave (Figure 4). Clinozoisite is present in trace amounts and is often found near pyroxenes. A thin rind of amphibole often rims the carbonate-bearing quartzite enclaves, indicating reaction between the pyroxenes and the tonalite.

The second group of light enclaves are enclaves with quartzo-feldspathic protoliths. These contain quartz (60%), alkali feldspar (>20 %), diopside (15%), biotite (<5%) and minor carbonate. These enclaves are more fine-grained than carbonate-bearing enclaves and show foliated texture, particularly when biotite is present.

A third category is comprised of light composite enclaves, which are dominated by quartz (35%), diopside (30%), alkali feldspar (20%), and minor carbonate and clinozoisite. Layers of varying mineralogy are visible in thin section. In several samples, a biotite rich layer is located close to the contact between the enclave and tonalite. Amphibole rich layers are also apparent, but they are located further from the contact. Except for areas that are biotite rich, light composite enclaves are fine-grained.

4.2 Geochemistry

4.2.1 Whole Rock Major Elements

The host tonalite is relatively homogeneous, at least on outcrop scale (20-30 m), and is characterized by 64-66 wt. % SiO_2, 1.5-2 wt. % MgO, 3-5 wt. % CaO, 6 wt. % FeO_T, 16 wt. % Al_2O_3 and total alkalis of ~5 wt. % (Figure 5).

By contrast, the enclaves show considerable major element heterogeneity. For example, SiO_2 contents range from 50 to 85 wt. %. For most major elements, there is considerable overlap between the two color types of enclaves although dark enclaves tend to be richer in Fe, Mg and Al and poorer in Si than light enclaves (Figure 5). Subtle but important differences between enclave subclasses are evident. Dark enclaves rich in biotite are very similar in composition to the host tonalite for most major elements, e.g., MgO, FeO_T, SiO_2, Na_2O and Al_2O_3. K_2O contents of three biotite-rich dark enclaves are much higher than in tonalite, but it is noteworthy that two biotite-rich samples have K_2O contents indistinguishable from tonalite. The amphibole-rich dark enclaves have similar MgO and FeO_T contents as tonalite, but have slightly higher CaO contents and much more variable SiO_2, Al_2O_3 and alkalis. Composite dark enclaves show compositional characteristics intermediate between biotite-rich and amphibole-rich dark enclaves with the exception of two with CaO contents as high as 10 wt. % (Table 4).

Light enclaves with quartzo-feldspathic protoliths (containing alkali feldspar) are compositionally similar to the tonalite and the biotite-rich dark enclaves. Light enclaves containing carbonates are enriched in Si and poor in Al, Fe, Mg and alkalis. SiO_2 contents range up to 88 wt. % (Table 5). Light enclaves in a CaO versus SiO_2 plot appear to fall along mixing trends between quartz and calcite with a small contribution from K-Al bearing phases like biotite and alkali feldspar (Figure 5). Composite light enclaves, which contain feldspar-bearing and

carbonate-bearing zones, have bulk compositions similar to tonalite and biotite-rich enclaves, with some showing correlated enrichments in K_2O and Al_2O_3 due to the presence of biotite and alkali feldspar.

Many of these similarities and differences can also be seen in a ternary diagram of Na+K, Ca+Mg, and Al (Figure 6). Here, it can be seen that biotite-rich dark enclaves and light enclaves of pelitic origin have similar compositions to tonalite. There appears to be a trend towards calcite displayed by the light enclaves as well as by the amphibole-rich and composite dark enclaves. Also displayed in the biotite-rich dark enclaves is a mixing trend with alkali feldspar.

For comparison, we have also plotted the major element compositions of mafic enclaves from the Sierra Nevada. These show some differences between the Peninsular Ranges Batholith dark enclaves and Sierra Nevada mafic enclaves. Generally, the mafic enclaves have less variable compositions. They have greater Fe and Mg contents than metasedimentary enclaves of all varieties and less Si (Figure 5). K_2O and CaO in mafic enclaves are more comparable to metasedimentary dark enclaves but still fall below a few metasedimentary dark enclaves. Na_2O in mafic enclaves are either comparable to or higher than that of metasedimentary enclaves.

4.2.2 Whole-rock trace elements

Enclaves

Trace element compositions in dark and light enclaves, normalized to bulk continental crust (BCC; Rudnick and Fountain, 1995), overlap in absolute and relative abundances. In general, trace element abundances of both dark and light enclaves are subparallel to BCC.

We first discuss the dark enclaves. Biotite-rich dark enclaves tend to have the highest concentrations of trace elements, with one of the biotite rich enclaves containing the highest rare earth element abundances of all the enclaves (Figure 7a). As expected, the biotite-rich enclaves contain the highest concentrations of large ion lithophile elements (LILEs), notably Rb and Ba. Those with the highest levels of Rb and Ba also have the highest REE abundances. Biotite-rich enclaves also have low Sr/Nd and CaO wt% (Figure 9a). The amphibolite enclaves generally have lower trace element abundances than the biotite-rich enclaves. Those with low K and Al have the lowest REE abundances. In figure 9a, samples with low K and Al have the highest CaO wt% and Sr/Nd. Those with high K and Al, due to the occurrence of biotite, have higher REE abundances and are intermediate between the low K and Al amphibolites and the biotite-rich enclaves. These samples are also characterized by low CaO and Sr/Nd (Figure 9a). The dark composite enclaves, which consist of discrete biotite-rich and amphibole-rich bands, share trace element characteristics intermediate between biotite-rich and amphibolite enclaves (Figure 7a). Two of the composite dark enclaves have high CaO wt% and Sr/Nd and low Ba, while the remaining four samples have lower CaO and Sr/Nd and higher Ba (Figures 9a, 9b).

As for the light enclaves, the carbonate-bearing quartzites contain the least amount of trace elements, which is somewhat expected because carbonates and quartz are known to be very

poor in trace elements (Figure 7b). Carbonate-bearing quartzite enclaves are characterized by high Sr/Nd and low Ba (Figures 9a, 9b). Most samples have similar abundance patterns compared to BCC with the exception of the most carbonate-rich samples, which are highly depleted in Rb and Ba and enriched in Sr (the most carbonate-rich samples have >2000 ppm Sr). The Sr/Nd ratios of all the carbonate-bearing samples are slightly to significantly higher than BCC and the quartzo-feldspathic enclaves. Quartzo-feldspathic enclaves are enriched in LILE and depleted in Sr. Light composite enclaves are similar in trace element abundance pattern to the metapelites, but their absolute abundances vary considerably (Figure 7b). In particular, the most trace element enriched samples show a pronounced depletion in Sr relative to Nd. Quartzo-feldspathic enclaves and light composite enclaves both have low Sr/Nd and high Ba (Figure 9b).

In summary, light and dark enclaves overlap almost completely in trace element composition. In detail, there are also similarities between the subgroups within the dark and light enclaves. Specifically, biotite-rich dark enclaves have trace element abundances that are similar between light composite enclaves and quartzo-feldspathic enclaves. Amphibolite and dark composite enclaves with low K and Al have trace element abundances similar to carbonate-bearing light enclaves.

Tonalite

The host tonalite has trace element abundances that overlap the biotite-rich enclaves. However, the tonalites have LILE contents intermediate between biotite-rich and amphibolite dark enclaves. The tonalite is distinctly richer in trace elements than the amphibolite enclaves (Figure 7a). We note that there are two clusters of tonalite compositions characterized by slightly different trace element abundances and subtle variations in abundance patterns as seen in different La/Yb (Figure 7b).

4.2.3 Mineral compositions

Biotite in biotite-rich dark enclaves, composite enclaves, and the host tonalite along with amphiboles in the amphibolite enclaves, carbonate-bearing light enclaves and the host tonalite were analyzed (SC-11, SC-7-2, SC-13 and SC-8-2, SC-7-2, SC-4-3 respectively). Major element compositions of all biotites, regardless of their host, are similar (Table 6). Trace element abundances of all biotites are generally similar with a few notable exceptions. Specifically, Cr, Sc, V and Ni contents in biotites from the dark enclaves are generally higher than those of their host tonalite. The overall trace element abundance patterns of the biotites, not surprisingly, are characterized by extreme depletions in REEs, Th and U, but show strong relative enrichments in the high field strength elements (HFSEs) like Nb, Ta, Zr and Hf (Table 6). We note, however, that the enrichment in HFSEs could be due to the presence of microscopic crystals of Fe-Ti oxide inclusions in the biotite, which could not be completely avoided during laser ablation analysis.

Amphibole compositions are shown in Table 7 and 8. Amphiboles are much more enriched in trace elements than biotites. In particular, they are characterized by relative enrichments in MREE and HREE but depletions in LREEs and LILEs (Figure 10). The amphiboles are also characterized by strongly negative Eu anomalies. Like biotites, amphiboles in enclaves and the host tonalite have similar trace element abundances.

Mafic minerals provide important controls on the trace element abundances of both igneous and metasedimentary dark enclaves. In igneous enclaves, mafic minerals such as amphibole, biotite, and magnetite are reservoirs for trace elements. Enrichments of HREE in enclaves can be attributed to amphibole, which sequesters rare earth elements during the equilibration between dark enclaves and their host granitoid. (Barbarin, 1990; Dorais et al., 1990;

Donaire et al., 2005). Growth of other minerals can also affect the diffusion of trace elements (e.g. Mn and Zn in Fe-Ti oxides; HREE and P in apatite) from host granitoid to enclave (Blundy and Sparks, 1989; Wiebe, 1996). Mineral assemblage in metasedimentary enclaves plays a similar role in overall trace element abundances, which vary widely. A pronounced characteristic of biotite-rich enclaves is their abundance in LILE, a result of their high biotite modal abundance (Figure 7a, 10). The abundance of trace elements in amphibolite and dark composite enclaves is more heterogeneous than that of biotite-rich enclaves and varies as a function of how K and Al rich the enclaves are. Amphibole is abundant in REE but contains low LILE (Figure 10). Consequently, the amphibolite and composite enclaves that are more abundant in LILE are also more abundant in K and Al.

5. Discussion

5.1 Protolith lithologies for the various enclave types

The mineralogy of the enclaves depends on whole rock major element composition, which is a function of protolith composition and changes in composition associated with open-system processes, such as physical mixing or diffusion. The fact that the whole-rock major and trace element compositions overlap between the light and dark enclaves suggest that they might have had similar protoliths, but have since experienced varying degrees of thermal metamorphism and chemical equilibration with the host tonalite magma.

The light enclaves are probably the least modified and provide the temporally closest snapshot of the original composition and mineralogy of the protolith. For example, the carbonate-bearing quartzite enclaves have major element compositions that can be explained by physical mixing of calcite and quartz. In some cases, the calcite is preserved, but in most cases the calcite has reacted with quartz to form wollastonite. Biotite- and alkali feldspar-bearing light enclaves are similar in major element composition to shales and can be classified as quartzo-feldspathic. The light composite enclaves contain distinct bands of quartzo-feldspathic and carbonate-rich layers, which can be explained as original compositional layering in the protolith. In some of these samples, the carbonate has reacted with quartz and biotite to form diopside (Figure 4).

Dark enclaves can also be distinguished by protolith type. For example, the amphibolite enclaves are similar in major element composition to the carbonate bearing light enclaves even though the amphibolites do not contain carbonate. Those amphibolites with high K and Al, due

to the presence of small amounts of biotite, may have had a feldspar rich component in their protoliths. Biotite-rich enclaves are similar in major element compositon to the light quartzo-feldspathic enclaves. However, the strongest evidence that the protoliths of the dark enclaves are metamorphic rocks, not magmas, is the presence of compositional banding in the composite dark enclaves.

The mineralogic changes can be explained by a combination of closed system thermal metamorphism and open system metamorphism. Based on our petrographic analyses, we envision the following sequence of reactions. Carbonate-bearing enclaves first undergo isochemical metamorphism involving decarbonation of carbonates to form wollastonite or diopside:

$$CaCO_3 + SiO_2 = CaSiO_3 + CO_2$$

$$CaMg(CO_3)_2 + 2SiO_2 = CaMgSi_2O6 + 2CO_2$$

This reaction appears to occur simultaneously throughout the enclave, consistent with closed system thermal metamorphism. Pyroxene formation is followed by amphibole formation, which begins first on the rims of the enclave, suggesting that the mineralogy is controlled by spatial variations in the composition of the system as a result of open-system mass exchange. For example, one open-system reaction is:

$$2CaMgSi_2O_6 + 3MgO + 4SiO_2 + H_2O = Ca_2Mg_5Si_8O_{22}(OH)_2$$

where MgO, SiO_2 and H_2O are assumed to be activities of these components within a fluid phase. This reaction shows that increased MgO, SiO_2 or H_2O activity will enhance amphibole formation at the expense of diopside. One possibility is that the CO_2 liberated from the above

decarbonation reactions gradually diffuses into the tonalite host while H_2O in the tonalite diffuses into the enclave. This results in an increase in H_2O activity (with decreasing CO_2 activity) in the enclave, beginning from the rim and eventually penetrating the enclave interior, after which all diopside is reacted to form amphibole. The last stage in our sequence is the formation of biotite from amphibole. This requires the introduction of K_2O, which, in the case of the carbonate-bearing quartzites, derives from the tonalite. We envision the following open system reaction:

$$6\ Ca_2Mg_5Si_8O_{22}(OH)_2 + 5Al_2O_3 + 5K_2O + 4H_2O = 10KMg_3AlSi_3O_{10}(OH)_2 + 12CaO + 18SiO_2$$

These concepts can be visualized in Figure 11a, where reactions and stability fields are expressed graphically in the form of activity diagrams at constant temperature and pressure (Helgeson et al., 1969; Brown and Essene, 1985; van Marcke de Lummen and Verkaeren, 1986; Dyer et al., 2011). For example, increasing SiO_2 and H_2O activity promotes reaction of diopside to amphibole. Increasing K_2O and decreasing CaO activity promote reaction of amphibole to biotite, whereas a decrease in Al_2O_3 and H_2O activity increases the stability field of amphibole relative to biotite at a given pressure and temperature. Similar concepts apply to the transformation of quartzo-feldspathic enclaves into biotite-rich dark enclaves. Alkali feldspar can react with Mg and water to form biotite, either isochemically if the enclave already has Mg and H_2O or through open system introduction of Mg and H_2O (Fig. 11b):

$$KAlSi_3O_8 + 3MgO + H_2O = KMg_3AlSi_3O_{10}(OH)_2$$

The end-product is a biotite-rich dark enclave. Additional reactions observed include the formation of clinozoisite from plagioclase and the formation of titanite by reaction of Fe-Ti oxides with carbonate or wollastonite, but these reactions are of lesser importance than the above-described reactions.

5.2 Similarities and differences between dark igneous and metasedimentary enclaves

Given the very similar macroscopic similarities between the dark enclaves of metasedimentary origin investigated here to mafic enclaves typically considered to be of magmatic origin, it is worth now examining how igneous and metasedimentary enclaves compare geochemically. For this comparison, we use mafic enclaves from the Sierra Nevada Batholith, which have been interpreted to represent mafic magma fragments entrained in a more felsic magma (Barbarin et al., 1989). These "igneous" enclaves are plotted on the same major element diagrams as the metasedimentary enclaves in Figures 5 and 6. It can be seen that many of the dark enclaves have broadly similar major element compositions as the Sierran mafic enclaves. For example, although SiO_2 contents of the dark metasedimentary enclaves are highly variable, many of the biotite-rich and composite dark enclaves have SiO_2 contents between 53-63 wt. %, within the range of Sierran mafic enclaves (45-65 wt. %). Similarly, there are overlaps in CaO, Na_2O, K_2O, and Al_2O_3 contents. We also note some similarities in trace elements. Sierran mafic enclaves and the dark metasedimentary enclaves are enriched in transition metals, such as Sc, Cr and Zn, relative to the tonalite. Sr/Nd ratios, which are a potentially useful tracer for carbonate-bearing protoliths because of the strong preference of Sr for carbonates, also show some overlap (Figure 9a). The composition of North American Shale Composite is also shown in order to illustrate the similarities between the shale and light sedimentary enclaves.

There are, however, differences. Many of the dark metasedimentary enclaves have SiO_2 contents > 70 wt. %, far higher than the Sierran mafic enclaves. Dark sedimentary enclaves tend to be slightly lower in Mg and Fe compared to the Sierran mafic enclaves. Al_2O_3 contents in some of the dark enclaves are >20 wt. %, which is higher than the Sierran mafic enclaves. The most Ca-rich of the dark metasedimentary enclaves are considerably richer in CaO than the Sierran mafic enclaves. Sr/Nd ratios in these Ca-rich dark metasedimentary enclaves are ~10 times higher than Sierran mafic enclaves. Ba contents of the dark biotite-rich metasedimentary enclaves are 4 times higher than the most Ba-rich Sierran mafic enclave.

Further trace element differences exist. Dark igneous enclaves have a pronounced enrichment in trace elements relative to their host granitoids, a feature that is not apparent in metasedimentary enclaves (Figure 8). The enrichment of REE in dark igneous enclaves is often explained by the diffusive transfer of REE between enclaves and their host (Orsini et al., 1991; Blundy and Sparks, 1992; Tepper and Kuehner, 2004). In particular, minerals that are abundant in the dark enclaves, such as amphibole or magnetite, equilibrate with the host and sequester the REEs (Ryerson and Hess, 1978; Allen, 1991; Blundy and Sparks, 1992). Most metasedimentary enclaves do not have host normative enrichments in REE as igneous enclaves have. Instead, they are characterized by enrichments in K and LILE, the extents of which vary as a function of mineralogy (Figures 7a, 8). High K and LILE metasedimentary enclaves are also characterized by having REE abundances that are similar to those of North American Shale Composite values (Taylor et al., 1981; Condie, 1993).

We note that, in terms of major elements, the Sierran mafic enclaves tend to fall on relatively narrow linear arrays, which supports a magmatic origin (Reid and Hamilton, 1987; Kumar and Rino, 2006). For example, in both Sierran mafic enclaves and their magma hosts,

Ca, Al, Fe, and Mg contents decrease with increasing Si (Dodge and Kistler, 1990; Chen and Williams, 1990; Barbarin et al., 1989). In contrast, the dark metasedimentary enclaves here do not show such coherent major element systematics. We expand on these concepts in the next section.

5.3 Using major element trends in dark enclaves to differentiate between igneous and metasedimentary origins

It is well-known that the major element compositions of cumulates, restites, and mafic magma fragments are complementary to their host granitoids, generating continuous linear to near-linear geochemical arrays (Reid and Hamilton, 1987; White and Chappell, 1977; Dodge and Kistler, 1990; Blundy and Sparks, 1992). For this reason, it seems likely that the major element trends seen in metasedimentary enclaves and their host tonalite might be readily distinguishable from the trends of igneous enclaves as discussed in the previous section. To explore this suggestion further in a more quantitative way, we modeled possible cumulates/restites derived from a granitoid magma. To insure applicability to our case study, we took the host tonalite composition of the Domenigoni Valley pluton as starting composition (see Table 3). We then used the thermodynamic program, known as MELTS (Ghiorso and Sack, 1995), to estimate possible cumulate/restite – liquid pairs. Given the high silica content of the Domenigoni Valley tonalite, we assume that fractional crystallization driven by gravitational segregation of crystals from residual liquid is highly inefficient, and thus, we assume batch equilibration of cumulate/restites with the residual liquid. To estimate different liquid fractions, our batch calculations were performed at temperatures between 720-960 °C for temperature intervals of

30 °C at a constant pressure of 1 kbar. This pressure was chosen because the magmatic equilibration pressures, estimated from Al in hornblende barometry (Schmidt, 1992) applied to our samples, was calculated to be 1-2 kbar.

As expected, cumulates/restites are richer in MgO, FeO_T, and CaO and lower in Na_2O and K_2O then the residual liquid (Figure 12). Given the simplicity of our calculations and our assumption of a very specific composition for a given plutonic system, there is a remarkable similarity between the our calculated cumulates/restites and the Sierran mafic enclaves, corroborating previous suggestions that such enclaves are indeed of magmatic origin. K_2O, however, is an exception. K_2O contents of Sierran mafic enclaves are much higher than the predicted cumulate/restite compositions. One possible explanation is that the K_2O content of our starting composition is not high enough to stabilize biotite in the cumulate/restite; we note that the K_2O content of our starting composition is lower than most of the Sierran mafic enclaves. However, it seems unlikely that any cumulates/restites with K_2O contents >3 wt. %, as seen in the most K-rich Sierran mafic enclaves, could ever be generated by igneous processes unless an unusually K-rich system is involved.

In Figure 12, we have also plotted the dark metasedimentary enclaves for comparison. It can be seen that these dark metasedimentary enclaves deviate in terms of CaO and K_2O and to a lesser extent SiO_2. We note that although it does not seem possible to generate K-rich cumulates/restites by crystallization of typical Sierran or Peninsular Ranges Batholith-type granitoids, it is possible from quartzo-feldspathic metasediments. Thus, although some of the Sierran mafic enclaves may be explained as igneous cumulates/restites, a small fraction, such as the K-rich ones, might have a metasedimentary origin.

Alternatively, Sierran mafic enclaves may represent the liquid portion of a crystallizing pluton. Again, using MELTS, we have calculated the composition of residual liquid from a fractionally crystallizing continental arc basalt (compositions from Kelemen et al., 2003). Continuous fractional crystallization from 1200 °C to 740 °C was kept at a constant 1 kbar to be consistent with MELTS calculations done in a batch crystallization model. In figure 13, it is possible to see the overlap of major element compositions of Sierran mafic enclaves with those of the modeled liquid compositions. Similarly, some metasedimentary dark enclaves show major element overlap with MELTS liquid compositions, particularly in FeO_T, MgO, K_2O, and Al_2O_3 concentrations.

In summary, we conclude that deviations from defined igneous arrays in terms of major element systematics may be the best way to differentiate mafic enclaves of metasedimentary origin from those of true igneous origin. The more scattered major element systematics of the metasedimentary enclaves are most certainly related to heterogeneity of their protoliths, and in the case of the Domenigoni Valley pluton, these enclaves have been arrested in various stages of chemical equilibration with the host magma, thereby preserving much of this heterogeneity. Had these enclaves resided longer in the magma chamber, allowing for further chemical equilibration, would the chemical systematics have approached those of the Sierran mafic enclaves, thereby masking the true extent of metasedimentary contribution to the formation of mafic enclaves.

6. Conclusions

Major and trace element characteristics provide us with the necessary diagnostic features to distinguish metasedimentary dark enclaves from igneous dark enclaves. The following criteria are outlined for metasedimentary dark enclaves: 1) The major element compositions of enclaves lack linear continuity with their granitoid host. Instead, mineralogy and major element compositions are controlled by the protolith lithology 2) With the influx of H_2O, biotite can crystallize provided the sedimentary protolith of an enclave is rich in K-feldspar, while amphibole can form from a carbonate rich protolith. 3) Trace element abundances in metasedimentary dark enclaves can vary significantly. Enclaves with carbonate rich protoliths have lower REE abundances, while enclaves with quartzo-feldspathic protoliths have higher REE abundances. 4) The abundance of trace elements in a mafic mineral is dependent on the modal proportion of that mineral in enclaves.

As demonstrated, the compositional and physical similarities between igneous and metasedimentary dark enclaves make it difficult to distinguish the two. This suggests that the origins of all dark enclaves should not be limited to just mafic magmas, cumulates, or hybrid magmas. Because some dark metasedimentary enclaves have been overlooked as igneous enclaves, they may be worth revisiting. Dark enclaves lacking outcrop context of sediment metamorphism could be misidentified as having either basaltic or cumulate in origin. Therefore, this comprehensive look at dark enclaves with metasedimentary protoliths may provide as a tool for diagnosing enclave origins, the implications of which can have profound effects on understanding what kind of differentiation path a granitoid body takes.

References

Allen, C.M., 1991, Local equilibrium of mafic enclaves and granitoids of the Turtle pluton, southeast California: Mineral, chemical, and isotopic evidence: American Mineralogist, v. 76, p. 574–588.

Barbarin, B., 2004, Mafic Magmatic Enclaves and Mafic Rocks Associated with some Granitoids of the Sierra Nevada Batholith, California: Lithos, v. 80, p. 155–177.

Barbarin, B., 1990, Plagioclase Xenocrysts and Mafic Magmatic Enclaves in Some Granitoids of the Sierra Nevada Batholith, California: Journal of Geophysical Research, v. 95, p. 17747–17756.

Barbarin, B., Dodge, F.C.W., Kistler, R.W., Bateman, P.C., 1989, Mafic Inclusions, Aggregates, and Dikes in Granitoid Rocks, Central Sierra Nevada Batholith, California- Analytic Data: US Geological Survey Bulletin; 1899.

Blundy, J., and Sparks, R.S.J., 1992, Petrogenesis of Mafic Inclusions in Granitoids of Adamello Massif, Italy: Journal of Petrology, v. 33, p. 1039–1104.

Brown, P.E., and Essene, E.J., 1985, Activity Variations Attending Tungsten Skarn Formation, Pine Creek, California: The Gibbs Free Energy of mixing of natural silicate liquids; an expanded regular solution approximation for the calculation of magmatic intensive variables, v. 89, p. 358–369.

Chappell, B.W., 1995, Magma Mixing and the Production of Compositional Variation within Granite Suites: Evidence from the Granites of Southeastern Australia: Journal of Petrology, v. 37, p. 449–470.

Chen, Y.D., Price, R.C., White, A.J.R., 1989, Inclusions in three S-type granites from SE Australia: Journal of Petrology, v. 30, p. 1181-1218.

Chen, Y.D., and Williams, I.S., 1990, Zircon Inheritance in mafic inclusions form Bega Batholith Granites, Southeastern Australia: an ion microprobe study: Journal of Geophysical Research, v. 95, p. 17787–17796.

Condie, K.C., 1993, Chemical Composition and Evolution of the Upper Continental Crust: Contrasting Results from Surface Samples and Shales: Chemical Geology, v. 104, p. 1–37.

Didier, J., 1973, Granites and their Enclaves. The Bearing of Enclaves on the Origin of Granites, Amsterdam: Elsevier, 393 pp.

DePaolo, D.J., 1980, Trace Element and Isotopic Effects of Combined Wallrock Assimilation and Fractional Crystallization: Earth and Planetary Science, v. 53, p. 189–202.

Dodge, F.C.W., and Kistler, R.W., 1990, Some Additional Observations on Inclusions in the Granitic Rocks of the Sierra Nevada: Journal of Geophysical Research, v. 95, p. 17841–17848.

Donaire, T., Pascual, E., Pin, C., and Duthou, J.-L., 2005, Microgranular enclaves as evidence of rapid cooling in granitoid rocks: the case of the Los Pedroches granodiorite, Iberian Massif, Spain: The Gibbs Free Energy of mixing of natural silicate liquids; an expanded regular

solution approximation for the calculation of magmatic intensive variables, v. 149, p. 247-265.

Dorais, M., Whitney, J., and Roden, M., 1990, Origin of Mafic Enclaves in the Dinkey Creek Pluton, Central Sierra Nevada Batholith, California: Journal of Petrology, v. 31, p. 853–881.

Dyer, B., Lee, C.-T.A., Leeman, W.P., and Tice, M., 2011, Open-system Behavior during Pluton–Wall-rock Interaction as Constrained from a Study of Endoskarns in the Sierra Nevada Batholith, California: Journal of Petrology, v. 52, p. 1987–2008.

Eichelberger, J.C., Origin of andesite and dacite: evidence of mixing at Glass Mountain in California and at other circum-Pacific volcanoes: Bulletin of the Geological Society of America, v. 86, p. 1381-1391.

Frost, T., and Mahood, G., 1987, Field, chemical, and physical constraints on mafic-felsic magma interaction in the Lamark Granodiorite, Sierra Nevada, California: Geological Society of America Bulletin, v. 99, p. 272–291.

Garrity, C.P., and Soller, D.R., 2009 Database of the Geologic Map of North America; adapted from the map by J.C. Redd, Jr. and others (2005): U.S. Geological Survey Data Series 424 [http://pubs.usgs.gov/ds/424/].

Gastil, R.G., 1975, Plutonic zones in the Peninsular Ranges of southern California and northern Baja California: Geology, v. 3, p. 361–363.

Ghiorso, M., and Sack, R., 1995, Chemical and Mass Transfer Processes. IV. A Revised and Internally Consistent Thermodynamic Model for the Interpolation and Extrapolation of

Liquid-Solid Equilibria in Magmatic Systems at Elevated Temperatures and Pressures: The Gibbs Free Energy of mixing of natural silicate liquids; an expanded regular solution approximation for the calculation of magmatic intensive variables, v. 119, p. 197–212.

Gromet, L.P., and Silver, L.T., 1987, REE Variations Across the Peninsular Ranges Batholith: Implications for Batholithic Petrogenesis and Crustal Growth in Magmatic Arcs: Journal of Petrology, v. 28.

Helgeson, H., Brown, T., and Leeper, R., 1969, Handbook of theoretical activity diagrams depicting chemical equilibria in geologic systems involving an aqueous phase at one Atm and 0 to 300^{o}C: Freeman Cooper and Co., San Francisco.

Hibbard, M.J., 1995, Petrography to Petrogenesis : Macmillan USA.

Kelemen, P.B., Hanghoi, K., Greene, A.R., 2003, One View of the Geochemistry of Subduction-related Magmatic Arcs, with an Emphasis on Primitive Andesite and Lower Crust: Treastise on Geochemistry, Editor: Roberta L. Rudnick. Executive Editors: Heinrich D. Holland and Karl K. Turekian, v.3, p.593-659.

Kistler, R.W., Wooden, J.L., and Morton, D.M., 2003, Isotopes and ages in the northern Peninsular Ranges batholith, southern California: U.S. Geological Survey Open-File Report 03-489 03-489, 45 p.

Kumar, S., and Rino, V., 2006, Mineralogy and geochemistry of microgranular enclaves in Palaeoproterozoic Malanjkhand granitoids, central India: evidence of magma mixing, mingling, and chemical equilibration: The Gibbs Free Energy of mixing of natural silicate liquids; an expanded regular solution approximation for the calculation of magmatic

intensive variables, v. 152, p. 591–609.

Maas, R., Nicholls, I.A., and Legg, C., 1997, Igneous and Metamorphic Enclaves in the S-type Deddick Granodiorite, Lachlan Fold Belt, SE Australia: Petrographic, Geochemical and Nd-Sr Isotopic Evidence for Crustal Melting and Magma Mixing: Journal of Petrology, v. 38, p. 815–841.

Morton, D.M., 1999, Preliminary digital geologic map of the Romoland quadrangle, Southern California:.

Orsini, J.B., Cocirta, C., and Zorpi, M.J., 1991, Genesis of mafic microgranular enclaves through differentiation of basic magmas, mingling, and chemical exchange with their host granitoid magmas, *in* Didier, J. and Barbarin, B. eds., Enclaves and granite petrology, Elsevier, p. 625.

Phillips, G.N., Wall, V.J., Clemens, J.D., 1981, Petrology of the Strathbogie batholith: a cordierite-bearing granite: Canadian Mineralogist, v. 19, p. 47-64.

Poli, G., Tommasini, S., 1991, Model for the Origin and Significance of Microgranular Enclaves in Calc-alkaline Granitoids: Journal of Petrology, v. 32, p. 657-666.

Price, R.C., 1983, Geochemistry of a peraluminous granitoid suite from NE Victoria, SE Australia: Geochemica et Cosmochimica Acta, v. 47, p. 31-42.

Reid, J.B., and Hamilton, M.A., 1987, Origin of Sierra Nevadan granite: evidence from small scale composite dikes: The Gibbs Free Energy of mixing of natural silicate liquids; an expanded regular solution approximation for the calculation of magmatic intensive variables, v. 96, p. 441–454.

Rudnick, R. and Fountain, D., 1995, Nature and Composition of the Continental Crust: A Lower Crustal Persepective: Reviews of Geophysics, v.33, p. 267-309.

Ryerson, F.J., and Hess, P.C., 1978, Implications of liquid-liquid distribution coefficients to mineral-liquid partitioning: Geochimica et Cosmochimica Acta, v. 42, no. 6, p. 921–932, doi: 10.1016/0016-7037(78)90103-5.

Schmidt, M.W., 1992, Amphibole composition in tonalite as a function of pressure: an experimental calibration of the Al-in-hornblende barometer: The Gibbs Free Energy of mixing of natural silicate liquids; an expanded regular solution approximation for the calculation of magmatic intensive variables, v. 110, p. 304–310.

Taylor, S.R., McLennan, S.M., Armstrong, R.L., and Tarney, J., 1981, The Composition and Evolution of the Continental Crust: Rare Earth Element Evidence from Sedimentary Rocks: Philosophical Transactions of the Royal Society of London, v. 301, p. 381–399.

Tepper, J.H., and Kuehner, S.M., 2004, Geochemistry of Mafic Enclaves and Host Granitoids from the Chilliwack Batholith, Washington: Chemical Exchange Processes beween Coexisting Mafic and Felsic Magmas and Implications for the Interpretation of Enclave Chemical Traits: The Journal of Geology, v. 112, p. 349–367.

Tobisch, O., McNulty, B., Vernon, R., 1997, Microgranitoid enclave swarms in granitic plutons, central Sierra Nevada, California: Lithos, v. 40, p. 321-339.

Todd, V.R., Erskine, B.G., and Morton, D.M., 1988, Metamorphic and tectonic evolution of the northern Peninsular Ranges Batholith, southern California, *in* Ernst, W.G. ed., Metamorphism and crustal evolution of the western United States, Prentice Hall, Englewood

Cliffs, p. 894–937.

van Marcke de Lummen, G., and Verkaeren, J., 1986, Physicochemical study of skarn formation in pelitic rock, Costabonne peak area, eastern Pyrenees, France: The Gibbs Free Energy of mixing of natural silicate liquids; an expanded regular solution approximation for the calculation of magmatic intensive variables, v. 93, p. 77–88.

Vernon, R.H., 1990, Crystallization and Hybridism in Microgranitoid Enclave Magmas: Microstructural Evidence: Journal of Geophysical Research, v. 95, p. 17849–17859.

Wetmore, P.H., Herzig, C., Alsleben, H., Sutherland, M., Schmidt, K.L., Schultz, P.W., and Patterson, S.R., 2003, Mesozoic tectonic evolution of the Peninsular Ranges southern and Baja California, *in* Johnson, S.E., Paterson, S.R., Fletcher, J.M., Girty, G.H., Kimbrough, D.L., and Martin-Barajas, A. eds., Tectonic evolution of northwestern Mexico and the southwestern USA, Geological Society of America, p. 93–116.

White, A.J.R., and Chappell, B.W., 1977, Ultrametamorphism and Granitoid Genesis: Tectonophysics, v. 43, p. 7–22.

Wiebe, R.A., Smith, D., Sturm, M., King, E.M., Seckler, M.S., 1997, Enclaves in the Cadillac Mountain Granite (Coastal Maine): Samples of Hybrid Magma from the Base of the Chamber: Journal of Petrology, v. 38, p. 393-423.

Figure Captions

Figure 1. Schematic cartoon for two different mechanisms of enclave formation. a) Dark enclaves from the Sierra Nevada Batholith are igneous in origin and likely formed by the fragmentation of mafic magmas intruded into felsic magma. b) A dark metasedimentary enclave from the Peninsular Ranges Batholith is hosted by tonalite and formed by the entrainment of wall rock fragments in a stoping pluton body. Both enclaves are angular and mafic-mineral rich.

Figure 2. Geologic map of the Domenigoni Valley Pluton. This region is located in the northern Peninsular Ranges Batholith (PRB). The pluton intrudes Mesozoic sediments, notably quartzite interbedded with carbonate-bearing layers, greywackes, and phyllites (from Morton, 1999).

Figure 3. Map of Cretaceous plutons along the western margin of North America (from Garrity and Soller, 2009).

Figure 4. Thin sections of enclaves (E) in contact the with host tonalite (T), arranged from least to most metamorphosed. On the left column, metamorphism of carbonate-bearing quartzite progresses to an amphibolite dark enclave. On the right column, quartzo-feldspathic enclaves progress towards biotite-rich enclaves. The middle column shows that light composite enclaves contain feldspar-bearing and carbonate-bearing layers, while dark composite enclaves preserve layers that are either biotite or amphibole rich. Mineral assemblages and their modal proportion are given for each enclave sample. Qz=Quartz, Cc=Calcite, Do=Dolomite, Wo=Wollastonite, Di=Diopside, Am=Amphibole, Bt=Biotite, Pl=Plagioclase, Kf=K-Feldspar, Ox=Fe-oxides

Figure 5. Whole rock major element compositions of metasedimentary enclaves and the host tonalite. a) SiO_2 vs. CaO wt% b) MgO vs. FeO_T wt% c) Al_2O_3 vs. K_2O wt% d) SiO_2 vs. Na_2O wt%. The compositions of igneous enclaves from the Sierra Nevada are plotted in the orange fields. Mineral abbreviations are as follows: Qz=Quartz, Cc=Calcite, Am=Amphibole, Bt=Biotite, Pl=Plagioclase, Kf=K-Feldspar

Figure 6. Ca+Mg, Na+K, Al (cationic wt.%) ternary diagram. The shaded field represents enclaves from the Sierra Nevada Batholith. Mineral abbreviations are the same as in figure 5.

Figure 7. Trace element compositions of enclaves and the host tonalite. a) Tonalite and dark enclaves are plotted with carbonate-bearing and quartzo-feldspathic enclaves represented by the two shaded regions in the background. b) Trace element abundances of light enclaves with dark enclaves in the shaded region. Samples are normalized to bulk continental crust (Rudnick and Fountain, 1995). Large ion lithophile elements are on the left, and rare earth elements from left to right are in order of decreasing ionic radius.

Figure 8. Host-normative trace elements of metasedimentary dark enclaves and Sierra Nevada enclaves. Trace element compositions of metasedimentary dark enclaves from the Peninsular Ranges are normalized to their host tonalite. In the case of Sierra Nevada samples, enclaves are normalized to their respective host granitoid.

Figure 9. Sr/Nd vs. a) CaO wt% and b) Ba (ppm) Sierra Nevada enclaves are represented by the orange shaded field. Sr/Nd is on a log scale.

Figure 10. Trace element composition of mafic minerals in dark metasedimentary enclaves and host tonalite. Biotite was analyzed in the tonalite, biotite-rich, and dark composite

enclaves (SC-13, SC-11, SC-7-1). Amphibole was analyzed in the tonalite, amphibolite, and dark composite enclaves (SC-4-3, SC-8-2, SC-7-2).

Figure 11. Progression of metamorphic reactions in metasedimentary enclaves. a) 1. Quartz and carbonate rich enclave entrained in a tonalite host. 2. CO_2 is released as carbonate and quartz react to form diopside. 3. With the influx of H_2O, the enclave progresses towards amphibole rich mineralogy. 4. The diffusion of K from tonalite to enclave results in the formation of biotite. 5. More K allows biotite to form in the enclave. b) 1. Quartzo-feldspathic enclaves are rich in K-feldspar. 2. With the influx of H_2O and Mg, the enclaves progress towards biotite-rich content. Activity diagrams are based on the metamorphic reactions that take place in enclaves. For each metamorphic reaction, the equilibrium constant depends on the activities and stoichiometries of element oxides. The slopes of activity plot curves are determined by rearranging the activities written for a given reaction's equilibrium constant.

Figure 12. Major element comparison of cumulates and metasedimentary enclaves. MELTS is used to model the composition of cumulates in equilibrium with liquid, using the Domenigoni Valley Pluton host tonalite as the liquid's starting composition (See Table 3). Batch crystallization was simulated at a range of temperatures from 720 °C to 960 °C. Pressure was kept at a constant 1 kbar. This is consistent with the 1-2 kbar calculated using the Al-in-hornblende barometer for the host tonalite from Domenigoni Valley. The compositions of cumulates are calculated mineral compositions and proportions for the given temperature range. Unlike modeled cumulates, PRB metasedimentary enclaves lack the linear continuity of major element compositions from tonalite to enclaves.

Figure 13. Major element comparison of metasedimentary enclaves with the liquid residue of fractionally crystallized continental arc basalt. The starting composition of basalt comes from Kelemen, 2003. Continuous fractional crystallization from 1200 °C to 740 °C was kept at a constant pressure of 1 kbar.

Figure 1.

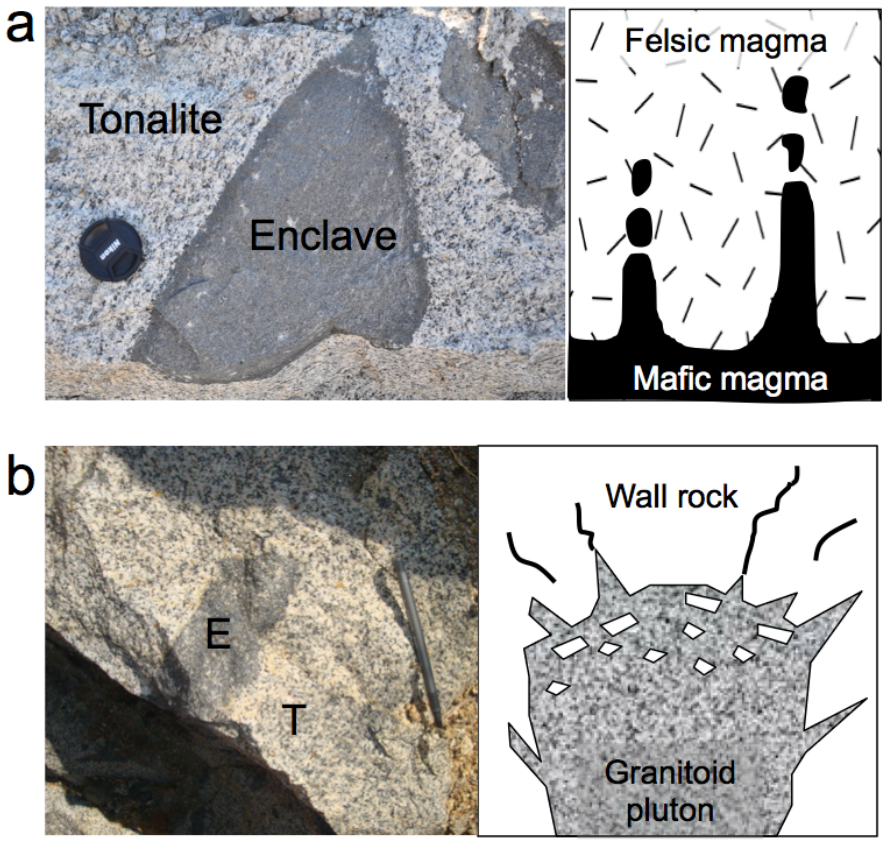
a
Tonalite
Enclave
Felsic magma
Mafic magma
b
E
T
Wall rock
Granitoid
pluton

Figure 2.

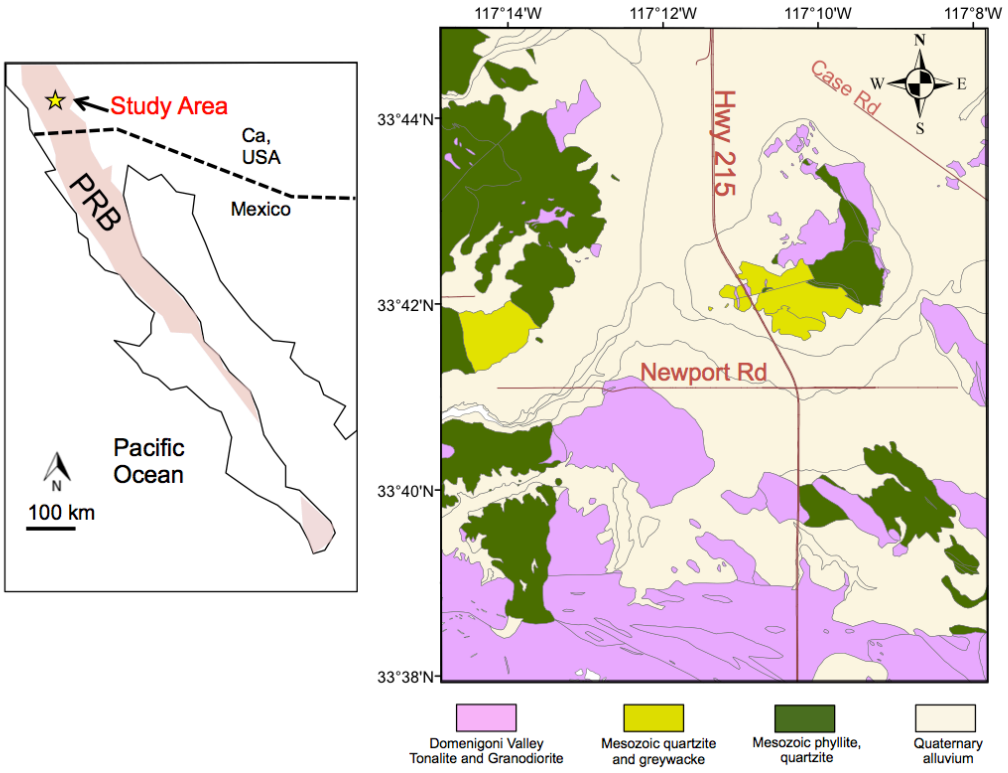
Study Area
Ca,
USA
Mexico
PRB
Pacific
Ocean
N
100 km
117°14'W
117°12'W
117°10'W
117°8'W
33°44'N
33°42'N
33°40'N
33°38'N
Hwy 215
Case Rd
Newport Rd
N
W
E
S
Domenigoni Valley
Tonalite and Granodiorite
Mesozoic quartzite
and greywacke
Mesozoic phyllite,
quartzite
Quaternary
alluvium

Figure 3.

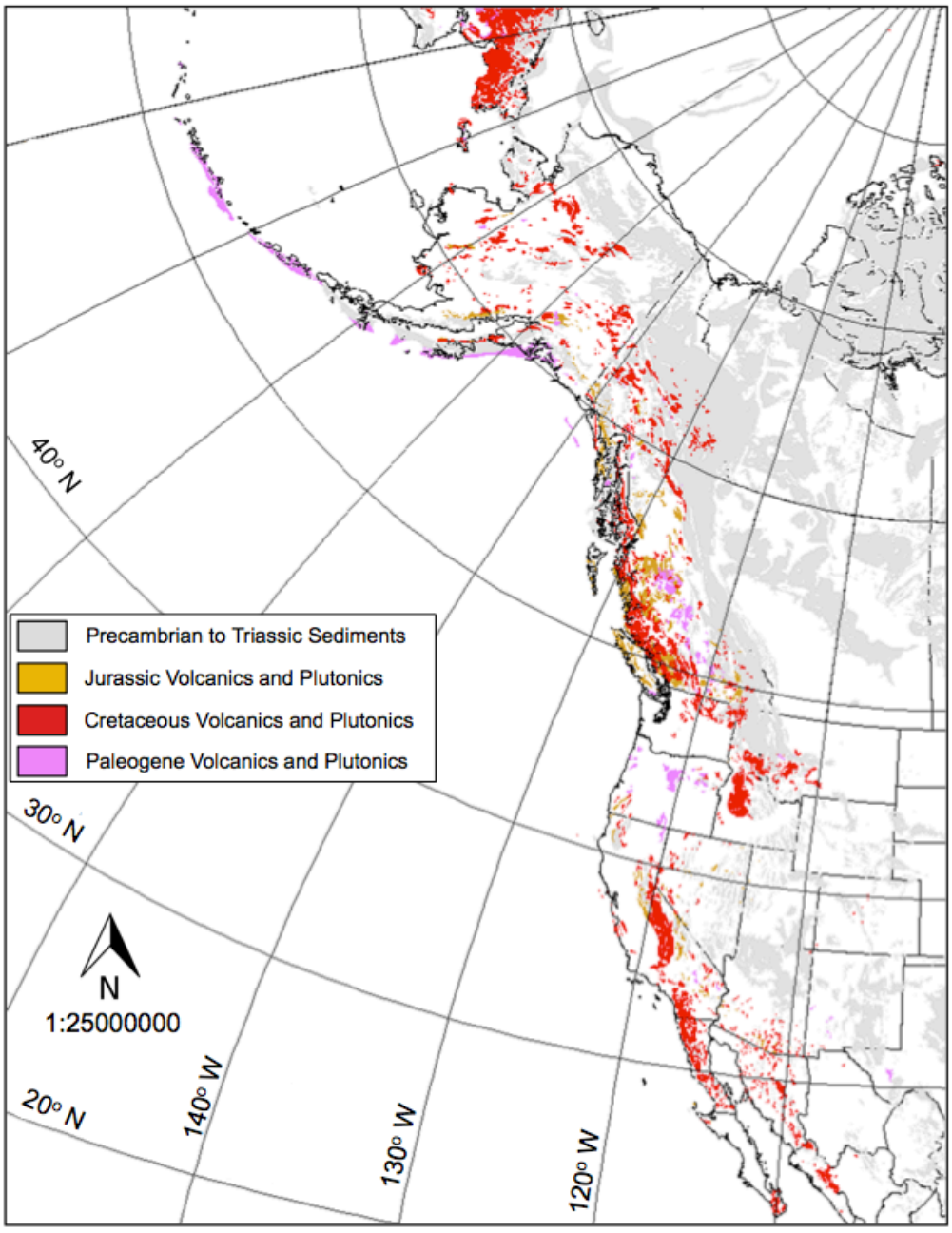
Precambrian to Triassic Sediments
Jurassic Volcanics and Plutonics
Cretaceous Volcanics and Plutonics
Paleogene Volcanics and Plutonics
40° N
30° N
20° N
140° W
130° W
120° W
N
1:25000000

Figure 4.

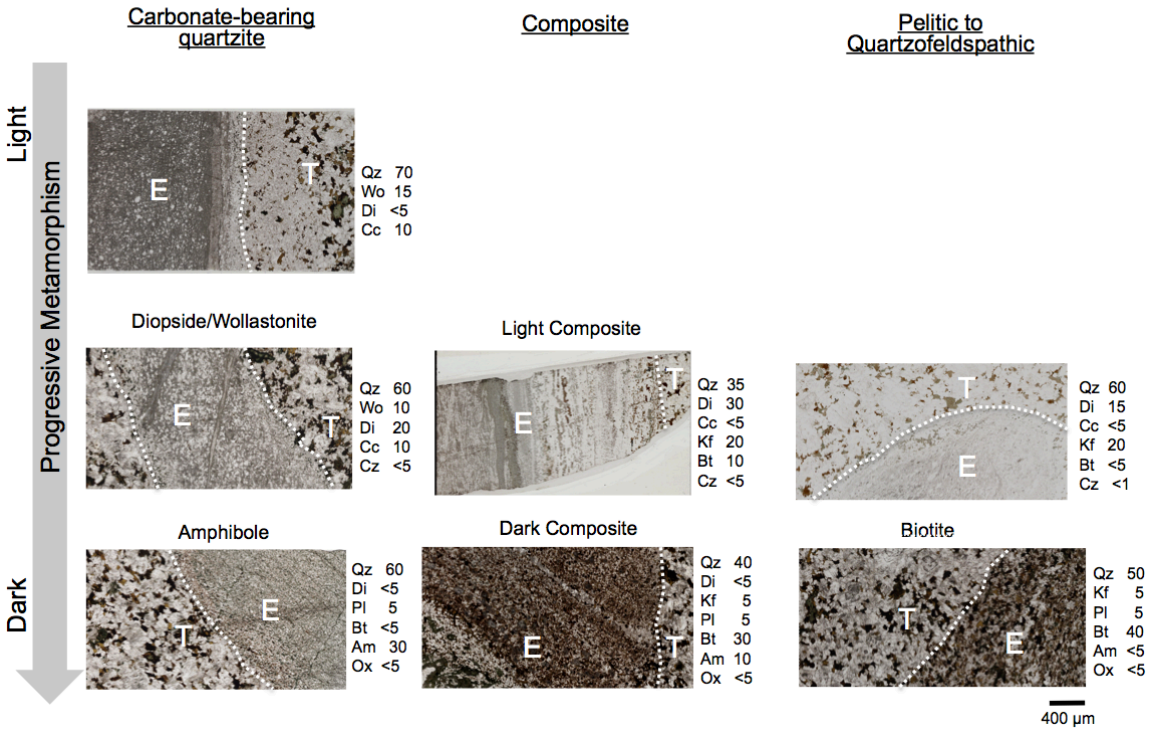
Carbonate-bearing quartzite
Composite
Pelitic to Quartzofeldspathic
Light
Progressive Metamorphism
Dark
E
T
Qz 70
Wo 15
Di <5
Cc 10
Diopside/Wollastonite
Qz 60
Wo 10
Di 20
Cc 10
Cz <5
Light Composite
Qz 35
Di 30
Cc <5
Kf 20
Bt 10
Cz <5
Qz 60
Di 15
Cc <5
Kf 20
Bt <5
Cz <1
Amphibole
Qz 60
Di <5
Pl 5
Bt <5
Am 30
Ox <5
Dark Composite
Qz 40
Di <5
Kf 5
Pl 5
Bt 30
Am 10
Ox <5
Biotite
Qz 50
Kf 5
Pl 5
Bt 40
Am <5
Ox <5
400 µm

Figure 5.

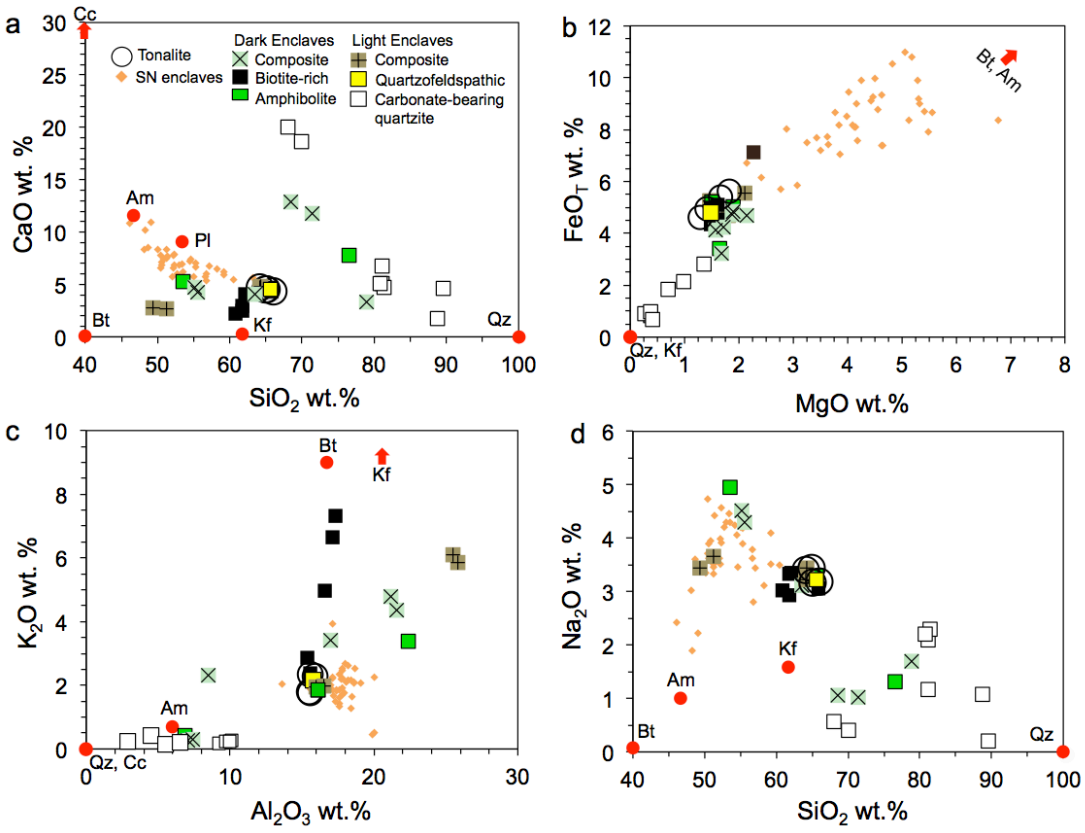
a
Cc
Tonalite
SN enclaves
Dark Enclaves
Composite
Biotite-rich
Amphibolite
Light Enclaves
Composite
Quartzofeldspathic
Carbonate-bearing quartzite
Am
Pl
Bt
Kf
Qz
CaO wt. %
SiO2 wt.%
b
Bt, Am
Qz, Kf
FeOT wt. %
MgO wt.%
c
Bt
Kf
Am
Qz, Cc
K2O wt. %
Al2O3 wt.%
d
Kf
Am
Bt
Qz
Na2O wt. %
SiO2 wt.%

Figure 6.

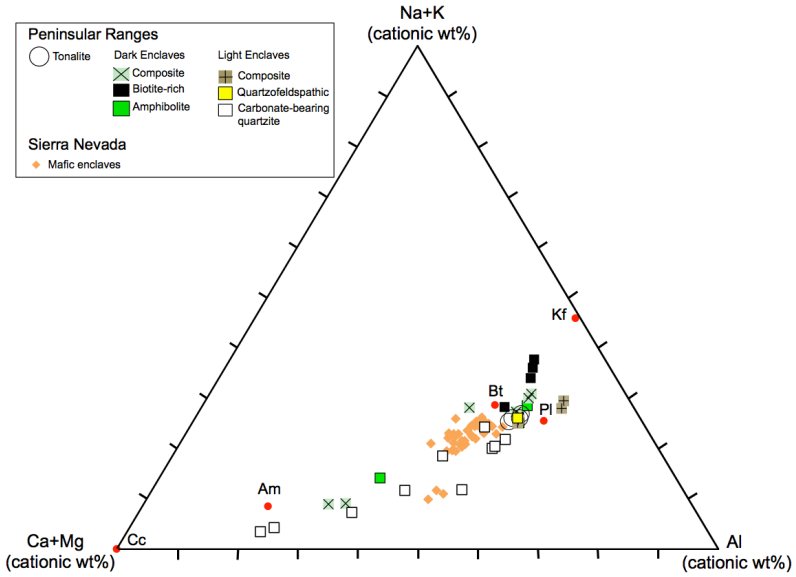
Peninsular Ranges
Tonalite
Dark Enclaves
Composite
Biotite-rich
Amphibolite
Light Enclaves
Composite
Quartzofeldspathic
Carbonate-bearing quartzite
Sierra Nevada
Mafic enclaves
Na+K
(cationic wt%)
Kf
Bt
Pl
Am
Cc
Ca+Mg
(cationic wt%)
Al
(cationic wt%)

Figure 7.

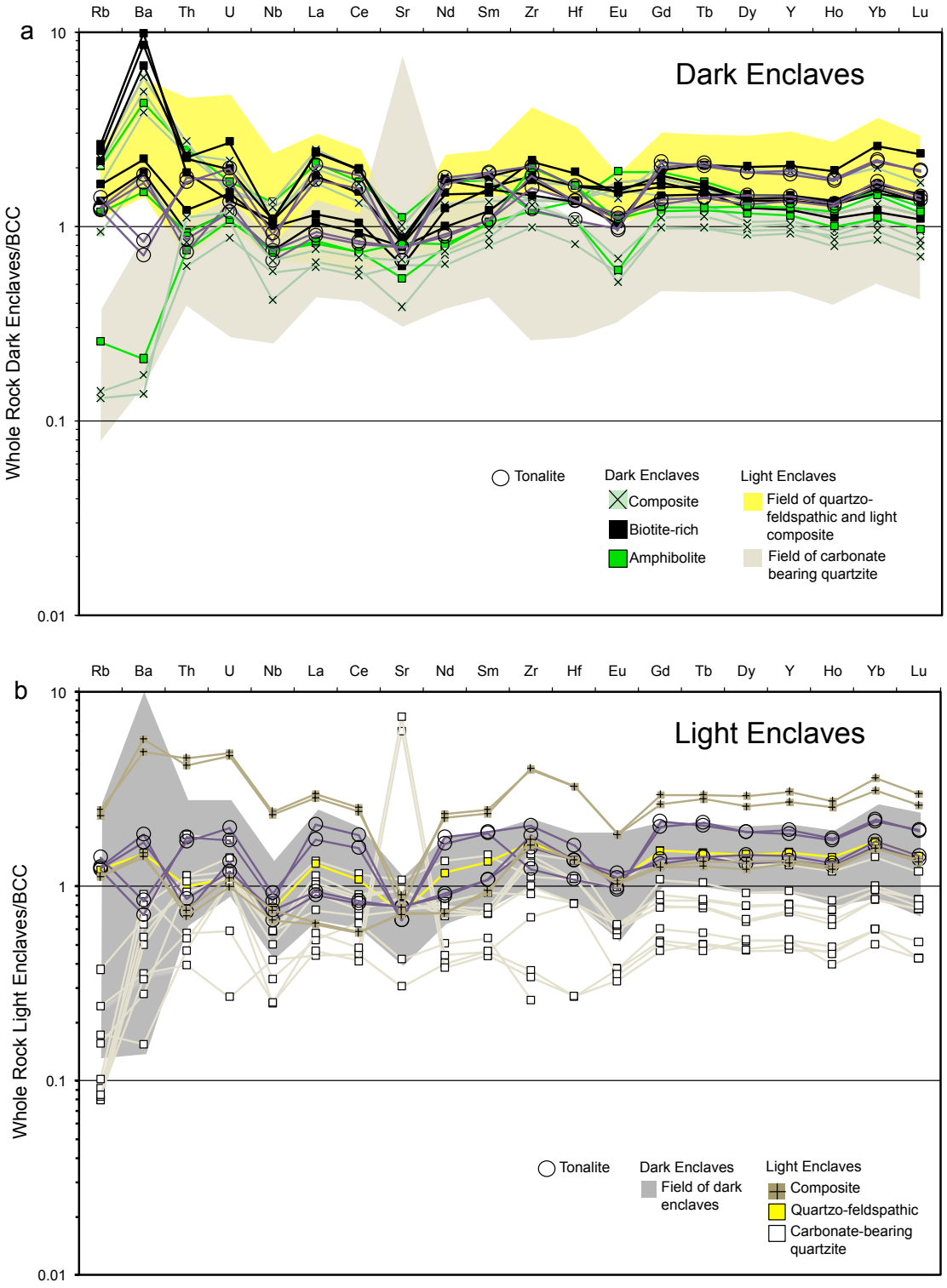
a
Rb Ba Th U Nb La Ce Sr Nd Sm Zr Hf Eu Gd Tb Dy Y Ho Yb Lu
10
1
0.1
0.01
Whole Rock Dark Enclaves/BCC
Dark Enclaves
Tonalite
Dark Enclaves
Composite
Biotite-rich
Amphibolite
Light Enclaves
Field of quartzo-feldspathic and light composite
Field of carbonate bearing quartzite
b
Rb Ba Th U Nb La Ce Sr Nd Sm Zr Hf Eu Gd Tb Dy Y Ho Yb Lu
10
1
0.1
0.01
Whole Rock Light Enclaves/BCC
Light Enclaves
Tonalite
Dark Enclaves
Field of dark enclaves
Light Enclaves
Composite
Quartzo-feldspathic
Carbonate-bearing quartzite

Figure 8.

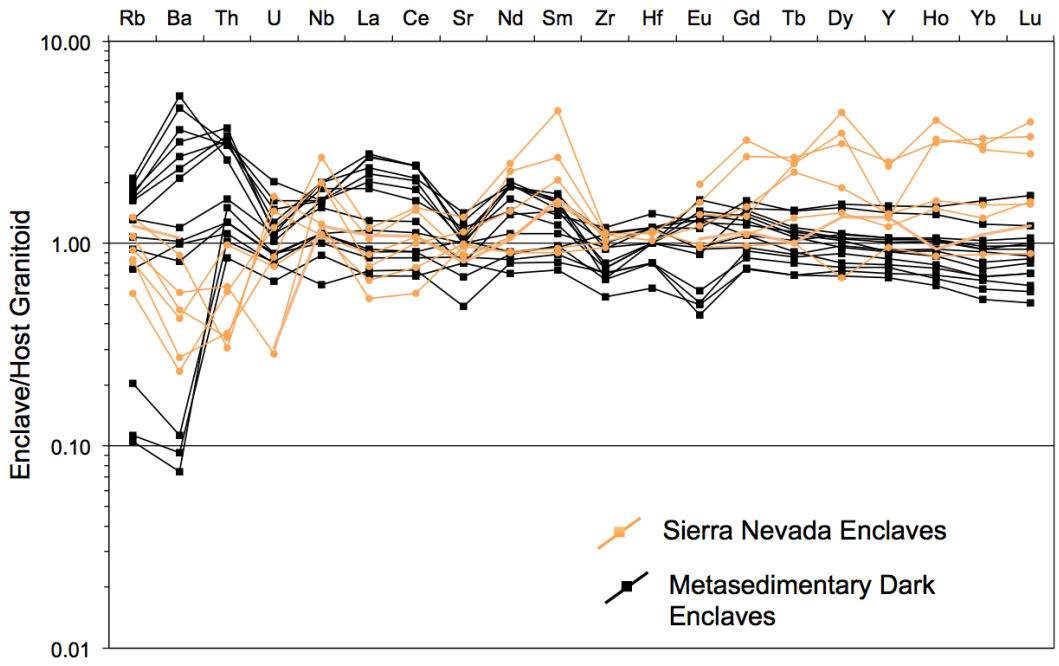
Rb
Ba
Th
U
Nb
La
Ce
Sr
Nd
Sm
Zr
Hf
Eu
Gd
Tb
Dy
Y
Ho
Yb
Lu
10.00
1.00
0.10
0.01
Enclave/Host Granitoid
Sierra Nevada Enclaves
Metasedimentary Dark Enclaves

Figure 9.

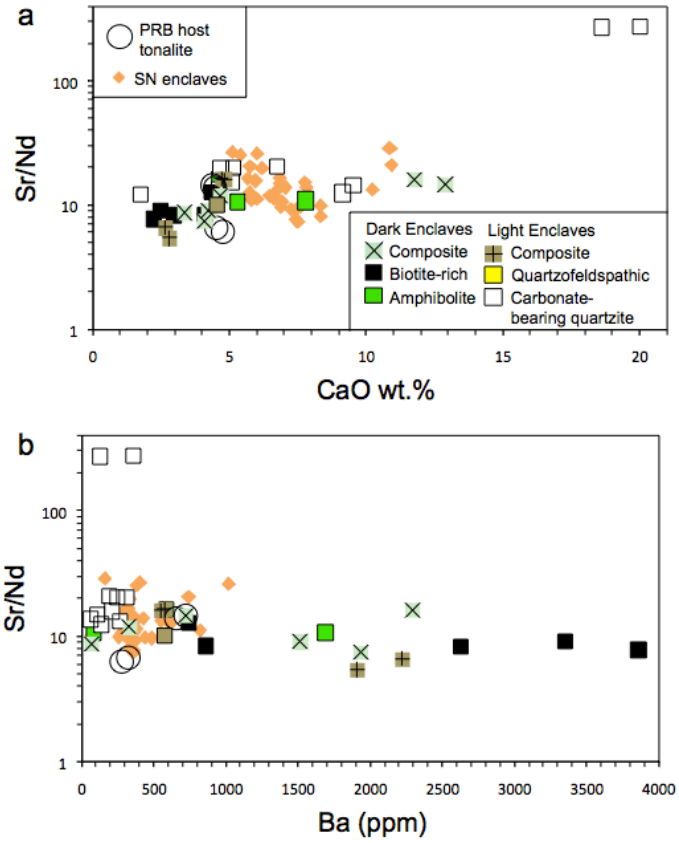
a
PRB host tonalite
SN enclaves
Dark Enclaves
Composite
Biotite-rich
Amphibolite
Light Enclaves
Composite
Quartzofeldspathic
Carbonate-bearing quartzite
Sr/Nd
CaO wt.%
b
Sr/Nd
Ba (ppm)

Figure 10.

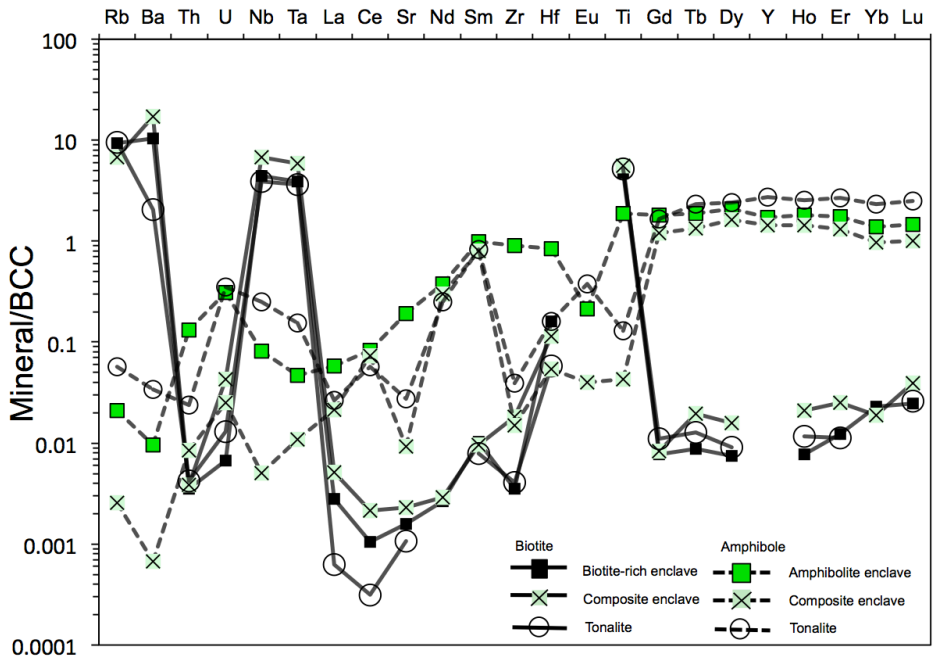
Rb Ba Th U Nb Ta La Ce Sr Nd Sm Zr Hf Eu Ti Gd Tb Dy Y Ho Er Yb Lu
100
10
1
0.1
0.01
0.001
0.0001
Mineral/BCC
Biotite
Biotite-rich enclave
Composite enclave
Tonalite
Amphibole
Amphibolite enclave
Composite enclave
Tonalite

Figure 11.

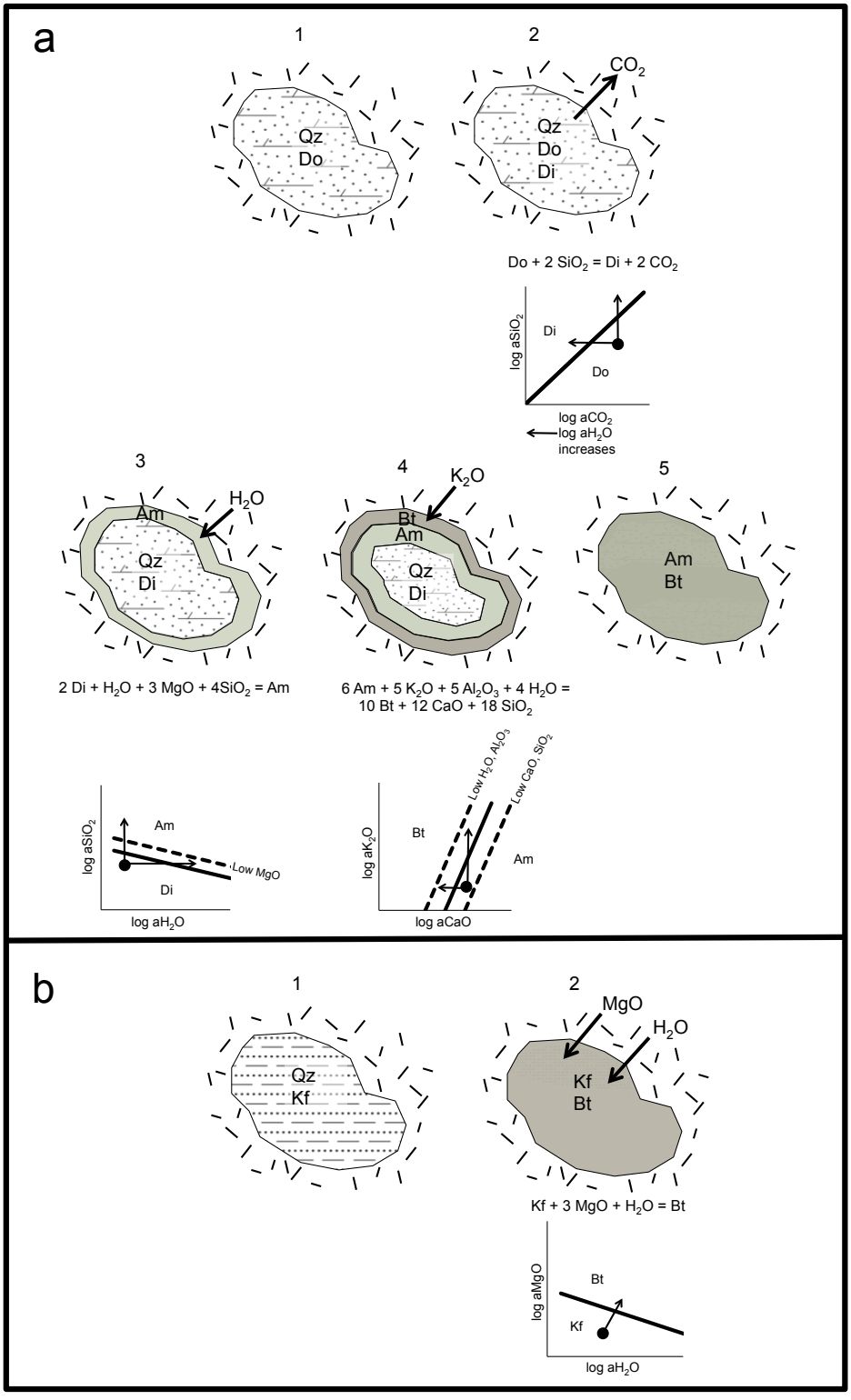
a
1
2
Qz
Do
CO2
Qz
Do
Di
Do + 2 SiO2 = Di + 2 CO2
log aSiO2
Di
Do
log aCO2
log aH2O
increases
3
4
5
H2O
Am
Qz
Di
K2O
Bt
Am
Qz
Di
Am
Bt
2 Di + H2O + 3 MgO + 4SiO2 = Am
6 Am + 5 K2O + 5 Al2O3 + 4 H2O =
10 Bt + 12 CaO + 18 SiO2
log aSiO2
Am
Low MgO
Di
log aH2O
log aK2O
Bt
Am
Low H2O, Al2O3
Low CaO, SiO2
log aCaO
b
1
2
Qz
Kf
MgO
H2O
Kf
Bt
Kf + 3 MgO + H2O = Bt
log aMgO
Bt
Kf
log aH2O

Figure 12.

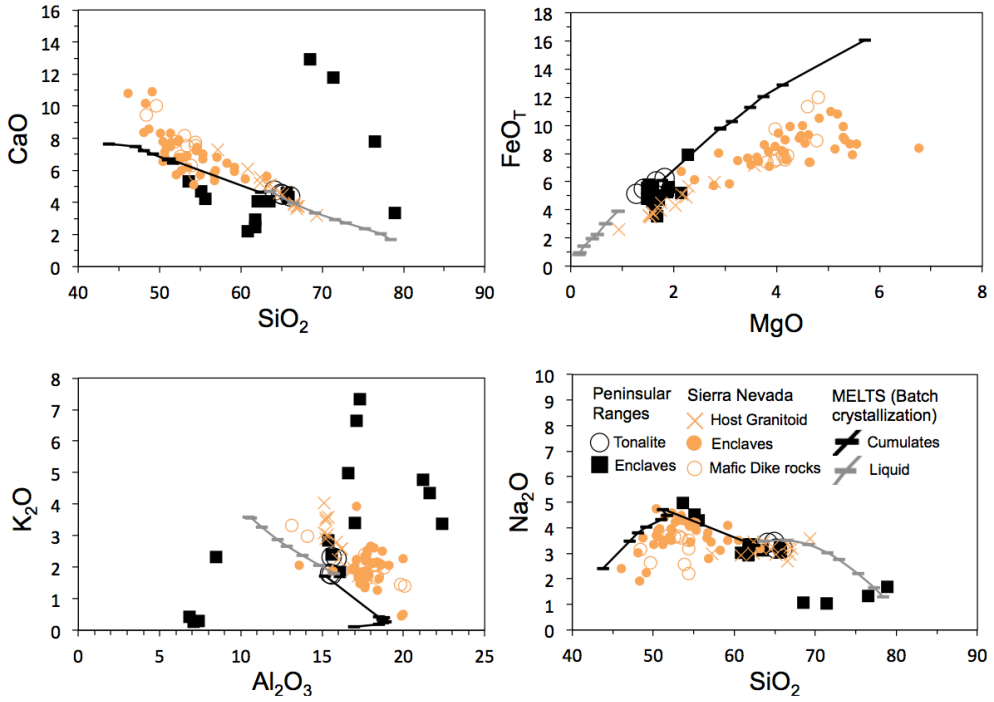
CaO
SiO2
FeOT
MgO
K2O
Al2O3
Na2O
SiO2
Peninsular Ranges
Tonalite
Enclaves
Sierra Nevada
Host Granitoid
Enclaves
Mafic Dike rocks
MELTS (Batch crystallization)
Cumulates
Liquid

Figure 13.

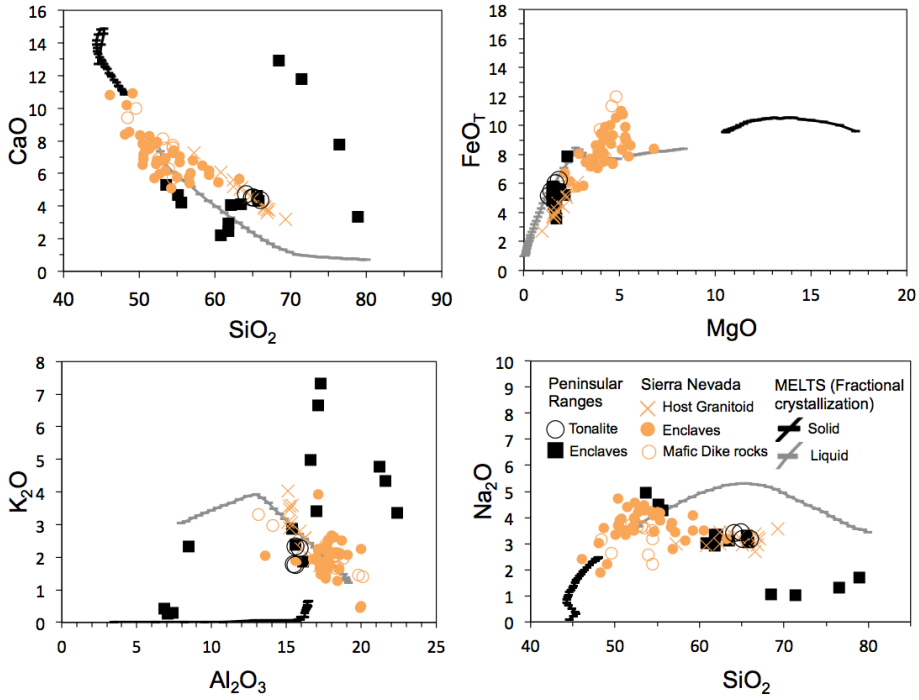
CaO
SiO2
FeOT
MgO
K2O
Al2O3
Na2O
SiO2
Peninsular Ranges
Tonalite
Enclaves
Sierra Nevada
Host Granitoid
Enclaves
Mafic Dike rocks
MELTS (Fractional crystallization)
Solid
Liquid

Table 1.

Enclave Type	Biotite-rich		Amphibolite		Dark composite	
Mineralogy	Mode %					
Quartz (Qz)	50		60		40-45	
Plagioclase (Pl)			5		0-5	
Alkali Feldspar (Kf)	5				5	
Biotite (Bt)	40		<5		30-40	
Amphibole (Am)	<5		30		5-30	
Fe-oxides (Ox)	<5		<5		<5	
Diopside (Di)			<5		<5	
Wollastonite (Wo)						
Calcite (Cc)						
Clinozoisite (Cz)						
		1 SD				
		n=5		n=3		n=6
SiO_2 (wt.%)	62.5	1.93	65.2	11.45	65.5	9.31
TiO_2	0.7	0.08	0.71	0.29	0.63	0.29
Al_2O_3	16.4	0.86	15.11	7.83	13.79	6.94
Cr_2O_3	0.01	0.01	0.02	0.01	0.02	0.01
FeO_T	6.44	1.36	5.63	1.23	5.31	0.75
MgO	0.09	0.03	0.09	0.02	0.1	0.04
MnO	1.69	0.33	1.68	0.2	1.82	0.2
CaO	3.21	0.95	5.91	1.67	6.84	4.3
Na_2O	3.14	0.19	3.19	1.82	2.62	1.58
K_2O	4.84	2.2	1.88	1.48	2.57	1.96
P_2O_5	0.17	0.02	0.18	0.01	0.16	0.02
Total	99.15		99.63		99.36	

Table 2.

Enclave Type	Carbonate-bearing		Quartzo-feldspathic		Light	
Mineralogy	Mode %					
Quartz (Qz)	60-80		60		35	
Plagioclase (Pl)	<5					
Alkali Feldspar (Kf)	0-5		20		20	
Biotite (Bt)	0-5		<5		10	
Amphibole (Am)	0-5					
Fe-oxides (Ox)						
Diopside (Di)	0-20		15		30	
Wollastonite (Wo)	0-30					
Calcite (Cc)	5-15		<5		<5	
Clinozoisite (Cz)	0-15		<1		<5	
		1 SD				
		n=8		n=1		n=4
SiO_2 (wt.%)	76.7	9	65.6		57.3	8.03
TiO_2	0.28	0.19	0.75		0.97	0.23
Al_2O_3	8.78	3.72	15.8		20.9	5.43
Cr_2O_3	<0.01	0	0.01		0.01	0
FeO_T	2.96	2.33	5.93		6.4	0.45
MgO	0.16	0.17	0.09		0.09	0.02
MnO	0.85	0.53	1.48		1.71	0.31
CaO	8.16	5.93	4.53		3.75	1.18
Na_2O	1.58	1.01	3.22		3.45	0.18
K_2O	0.46	0.58	2.16		1.44	2.32
P_2O_5	0.07	0.05	0.18		0.2	0.02
Total	100		99.75		96.22	

Table 3.

Sample Name	SC-13A	SC-13B	SC-13C	SC-13D
Sample Type	Tonalite	Tonalite	Tonalite	Tonalite
SiO_2 (wt%)	66.0	65.1	64.1	64.9
TiO_2	0.64	0.74	0.87	0.86
Al_2O_3	15.6	15.9	15.6	15.5
Cr_2O_3	<0.01	<0.01	<0.01	<0.01
FeO_T	5.69	6.09	6.94	6.68
MnO	0.1	0.11	0.14	0.13
MgO	1.28	1.42	1.82	1.66
CaO	4.39	4.50	4.74	4.55
Na_2O	3.19	3.17	3.41	3.45
K_2O	2.33	2.27	1.77	1.80
P_2O_5	0.16	0.16	0.29	0.30
Total	99.38	99.46	99.68	99.83
LOI	0.72	0.63	0.60	0.55
Rare Earth Element (ppm)				
Rb	72.5	71.3	70.3	81.1
Sr	255	251	217	217
Y	26.9	28.6	37.1	38.9
Zr	223	195	253	151
Nb	8	9	10	11
Ba	719	651	278	328
La	16.1	16.8	37.2	31.4
Ce	34	35.2	77.3	66.4
Nd	17.8	18.3	35.5	33.2
Sm	4.2	4.2	7.4	7.3
Eu	1.4	1.32	1.15	1.18
Gd	4.7	4.96	7.72	7.28
Tb	0.79	0.79	1.14	1.19
Dy	4.56	5.07	6.62	6.66
Ho	0.97	0.99	1.31	1.33
Yb	3.2	3.4	4.3	4.4
Lu	0.45	0.47	0.64	0.63
Hf	5	5	6	4
Th	4.1	4.8	10	9.5
U	1.9	1.69	2.44	2.84

Table 4.

Sample Name	SC-8A	SC-8B	SC-8C	SC-	SC-	SC-	SC-	SC-	SC-7A	SC-7B	SC-7C	SC-7D	SC-7E	SC-7F
Enclave type	Amphibolite	Amphibolite	Amphibolite	Biotite-rich	Biotite-rich	Biotite-rich	Biotite-rich	Biotite-rich	Composite	Composite	Composite	Composite	Composite	Composite
SiO_2 (wt%)	65.6	53.6	76.5	65.8	61.8	61.8	60.8	62.1	55.1	63.5	55.6	71.4	78.9	68.5
TiO_2	0.77	0.93	0.37	0.78	0.63	0.67	0.64	0.8	0.92	0.83	0.93	0.36	0.36	0.39
Al_2O_3	16.1	22.4	6.83	15.6	16.6	17.1	17.3	15.4	21.6	17	21.2	7.41	8.46	7.07
Cr_2O_3	<0.01	<0.01	<0.01	<0.01	<0.01	0.01	<0.01	0.01	0.03	0.01	0.02	<0.01	<0.01	<0.01
FeO_T	6.45	6.22	4.21	6.16	5.35	5.6	6.31	8.77	5.97	5.78	5.82	5.11	3.96	5.23
MnO	0.1	0.07	0.11	0.1	0.07	0.06	0.06	0.14	0.06	0.08	0.08	0.16	0.06	0.15
MgO	1.51	1.9	1.64	1.48	1.48	1.64	1.6	2.27	1.89	2.15	1.88	1.58	1.68	1.71
CaO	4.61	5.32	7.79	4.33	2.95	2.47	2.22	4.06	4.68	4.09	4.24	11.8	3.35	12.9
Na_2O	3.3	4.96	1.32	3.06	3.34	2.94	3.02	3.35	4.51	3.11	4.29	1.03	1.7	1.06
K_2O	1.86	3.37	0.42	2.39	4.98	6.65	7.33	2.86	4.35	3.4	4.78	0.29	2.32	0.28
P_2O_5	0.18	0.17	0.18	0.2	0.15	0.16	0.17	0.18	0.17	0.17	0.19	0.13	0.13	0.15
Total	100.48	98.94	99.37	99.9	97.35	99.1	99.45	99.94	99.28	100.12	99.03	99.27	100.92	97.44
LOI	0.51	1.04	0.78	0.54	3.3	0.4	0.92	1.13	0.79	0.79	0.66	1.33	0.48	2.73
Rare Earth Elements														
Rb (ppm)	68.3	118	14.7	78.2	125	141	153	95.6	122	94.7	130	8.2	54.2	7.6
Sr	265	363	175	255	282	265	269	204	307	253	328	205	125	218
Y	24.9	28.7	22.7	28.8	28.1	27.2	24.4	41.3	21.1	38.3	24.5	18.3	19.2	20.6
Zr	247	149	148	213	251	267	223	178	168	210	169	122	160	159
Nb	9	16	9	9	13	13	13	12	15	13	16	7	5	8
Ba	588	1690	81.2	740	2630	3360	3860	863	1930	1510	2290	66.4	718	53.6
La	15.1	38	14.7	18.7	43.4	32.7	42.9	20.8	30	35.6	44.6	11.1	11.8	13.7
Ce	30.9	71.3	30.9	38.6	82.2	63	82.8	43.9	55.3	69.2	81.8	23.4	25.2	29
Nd	16.2	34.2	15.8	20	34.3	29.6	34.8	24.7	25.8	33.8	36	12.7	14.3	14.9
Sm	4	6.7	4.1	4.7	7	5.8	6.2	6.1	5.2	7.4	6.8	3.1	3.4	3.7
Eu	1.31	2.3	0.71	1.34	1.83	1.79	1.92	1.24	1.85	1.67	2.02	0.7	0.62	0.82
Gd	4.51	6.87	4.31	5.18	6.57	5.79	6.08	7.02	5.14	7.62	6.42	3.53	3.55	4
Tb	0.7	0.95	0.68	0.82	0.92	0.9	0.85	1.16	0.72	1.14	0.88	0.55	0.55	0.63
Dy	4.44	5.09	4.09	5.08	4.86	4.81	4.37	7.13	3.65	6.86	4.7	3.15	3.34	3.48
Ho	0.91	1.01	0.76	1.03	1.01	0.99	0.84	1.47	0.73	1.35	0.89	0.6	0.68	0.65
Yb	2.9	3	2.2	3.3	3.1	3	2.4	5.2	2.2	4	2.6	1.7	2.1	1.9
Lu	0.39	0.42	0.32	0.48	0.44	0.45	0.36	0.78	0.32	0.55	0.38	0.23	0.28	0.26
Hf	6	5	4	5	6	7	6	5	5	6	5	3	4	4
Th	5.2	14	4.2	5.2	12.5	12.8	10.6	6.8	13.2	13.2	15.3	3.5	4.6	6.2
U	1.69	2.42	1.53	1.67	2.8	3.86	1.95	2.12	2.21	3.09	2.11	1.24	1.52	1.69

Table 5.

Sample	SC-1A	SC-1B	SC-1C	SC-1D	SC-3A	SC-3B	SC-5A	SC-5B	SC-	SC-16A	SC-16B	SC-16C	SC-16D
Enclave type	Carbonate-bearing	Carbonate-bearing	Carbonate-bearing	Carbonate-bearing	Carbonate-bearing	Carbonate-bearing	Carbonate-bearing	Carbonate-bearing	Pelitic	Light composite	Light composite	Light composite	Light composite
SiO_2 (wt%)	81.1	81.1	81.4	80.8	70	68	89.5	88.7	65.6	49.4	51.3	64.1	64.3
TiO_2	0.22	0.23	0.24	0.23	0.1	0.09	0.15	0.26	0.75	1.22	1.09	0.75	0.8
Al_2O_3	9.25	9.72	10.1	9.97	5.53	6.5	2.91	4.5	15.8	25.8	25.5	16	16.5
Cr_2O_3	<0.01	<0.01	<0.01	<0.01	<0.01	<0.01	<0.01	<0.01	<0.01	0.01	0.01	0.01	0.01
FeO_T	1.04	1.11	1.12	1.21	3.45	2.66	0.85	2.27	5.93	6.86	5.79	6.48	6.48
MnO	0.1	0.07	0.04	0.07	0.15	0.14	0.65	0.17	0.1	0.08	0.07	0.11	0.12
MgO	0.37	0.37	0.27	0.37	1.35	0.99	0.41	0.69	1.48	2.1	1.8	1.47	1.46
CaO	6.73	5.13	4.69	5.09	18.6	20	4.6	1.74	4.53	2.81	2.66	4.72	4.82
Na_2O	1.16	2.09	2.3	2.2	0.41	0.56	0.2	1.08	3.22	3.45	3.66	3.22	3.45
K_2O	0.19	0.25	0.28	0.23	0.16	0.22	0.25	0.41	2.16	5.84	6.11	1.94	1.99
P_2O_5	0.04	0.04	0.06	0.06	0.04	0.03	0.03	0.05	0.18	0.21	0.21	0.19	0.17
Total	100.2	100.11	100.5	100.23	99.79	99.19	99.55	99.87	99.75	97.78	98.2	98.99	100.1
LOI	0.65	0.5	0.44	0.41	0.37	1	1.2	0.55	0.47	1.7	1.69	0.59	1.79
Rare Earth Elements													
Rb (ppm)	4.6	5.3	4.6	4.8	70.3	4.9	5.9	10	14	143	134	65.4	64.4
Sr	309	283	311	245	236	2040	2420	136	98.5	106	101	24.1	24.4
Y	14.5	15	16.1	16.1	29.8	9.9	10.6	10.5	9.4	2.08	1.93	0.95	0.92
Zr	164	123	177	180	206	41.7	84.9	32	45.2	9.6	9.2	3.6	3.7
Nb	7	6	7	7	9	3	3	4	5	29	28	8	9
Ba	193	245	310	213	572	130	354	59.9	138	1910	2220	576	551
La	20.3	16.4	18.8	18.2	23.4	8.3	10.3	9.5	7.9	1.7	1.5	0.9	0.6
Ce	37.9	31.8	36.7	35.5	45.2	17.3	20.2	27.1	18.8	53.5	50.8	11.4	11.6
Nd	14.9	14	15.6	15.8	23.3	7.6	8.8	10.1	8	252	292	237	231
Sm	2.8	2.8	2.8	3	5.2	1.7	1.8	2.1	1.8	46.8	44.7	14.5	14.5
Eu	0.71	0.75	0.75	0.76	1.27	0.39	0.42	0.45	0.45	10.6	9.48	4.59	4.48
Gd	2.83	2.79	3.04	3.24	5.46	1.66	1.83	2.16	1.88	1.65	1.56	0.75	0.71
Tb	0.43	0.44	0.47	0.48	0.83	0.28	0.26	0.32	0.28	10.2	8.96	4.67	4.28
Dy	2.29	2.34	2.75	2.78	5.08	1.65	1.85	1.82	1.62	61.1	54.3	27.1	26.1
Ho	0.48	0.51	0.57	0.57	1.07	0.34	0.37	0.3	0.35	6.78	6.29	3.08	3.1
Yb	1.7	1.7	1.9	1.9	3.4	1.2	1.2	1	1.2	7.2	6.2	3.1	3.1
Lu	0.25	0.25	0.28	0.26	0.47	0.14	0.14	0.14	0.17	0.98	0.86	0.45	0.44
Hf	4	3	4	5	5	1	3	<1	1	2.22	2.2	1.26	1.23
Th	6.3	5.2	6.3	5.9	5.6	3.2	3	2.6	2.2	25.5	23.3	3.9	4.2
U	1.7	1.58	1.99	1.57	1.55	0.83	1.48	1.47	0.38	6.84	6.66	1.4	1.56

Table 6.

Sample	SC-7-1	SC-7-1	SC-7-1	SC-7-1	SC-7-1	SC-7-1	SC-7-1	SC-11	SC-11	SC-11	SC-11	SC-11	SC-11	SC-11
Enclave Type	Composite	Composite	Composite	Composite	Composite	Composite	Composite	Biotite-rich	Biotite-rich	Biotite-rich	Biotite-rich	Biotite-rich	Biotite-rich	Biotite-rich
No.	21	24	10	11	12	13	14	32	34	36	38	40	41	42
Location in	Tonalite	Tonalite	Tonalite	Tonalite	Enclave	Enclave	Enclave	Tonalite	Tonalite	Tonalite	Tonalite	Tonalite	Enclave	Enclave
SiO_2 (wt%)	39.8	37.9	37.3	38.1	38.4	39	38.2	37.8	37.6	37.7	36.7	37.2	35.4	34.7
TiO_2	3.62	3.54	3.82	2.65	3.87	3.4	3.82	2.89	3.19	3.83	3.59	3	3.44	4.38
Al_2O_3	16.7	16.5	18.9	18.2	17.5	16.6	18.7	18.6	15.2	14	15.8	14.2	16.2	16.2
Cr_2O_3	0.02	0.03	0.02	0	0.08	0.09	0.1	0.02	0.03	0.02	0.02	0.04	0.06	0.05
FeO_T	24.2	23.5	23.6	22.9	22.2	22.4	21	22.9	24.7	25.8	24.4	24.9	25	25.9
MnO	0.36	0.28	0.39	0.35	0.29	0.25	0.26	0.28	0.33	0.36	0.36	0.39	0.35	0.33
MgO	6.16	8.19	6.42	7.6	7.37	8.49	8.24	7.68	7.37	7.12	7.89	8.61	9.1	6.63
CaO	0.06	0.23	0.05	0.12	0.34	0.05	0.08	0.05	0.1	0.08	0.03	0.03	0.04	0.04
Na_2O	0.08	0.06	0.08	0.12	0.07	0.08	0.1	0.06	0.05	0.06	0.05	0.05	0.05	0.06
K_2O	9	9.72	9.5	9.88	9.63	9.66	9.51	9.68	11.4	11.1	11.3	11.6	10.4	11.7
Total	100	99.95	100.08	99.92	99.75	100.02	100.01	99.96	99.97	100.07	100.14	100.02	100.04	99.99
Number of ions on the basis of 10														
Na	0.01	0.01	0.01	0.02	0.01	0.01	0.01	0.01	0.01	0.01	0.01	0.01	0.01	0.01
Mg	0.61	0.82	0.64	0.76	0.73	0.84	0.81	0.76	0.75	0.73	0.8	0.88	0.93	0.69
Al	1.31	1.3	1.49	1.43	1.37	1.3	1.45	1.46	1.23	1.13	1.27	1.15	1.31	1.33
Si	2.65	2.55	2.49	2.54	2.55	2.59	2.52	2.52	2.57	2.59	2.51	2.56	2.42	2.41
K	0.76	0.83	0.81	0.84	0.82	0.82	0.8	0.82	0.99	0.97	0.98	1.02	0.9	1.03
Ca	0	0.02	0	0.01	0.02	0	0.01	0	0.01	0.01	0	0	0	0
Ti	0.18	0.18	0.19	0.13	0.19	0.17	0.19	0.15	0.16	0.2	0.19	0.16	0.18	0.23
Cr	0	0	0	0	0	0	0.01	0	0	0	0	0	0	0
Mn	0.02	0.02	0.02	0.02	0.02	0.01	0.01	0.02	0.02	0.02	0.02	0.02	0.02	0.02
Fe	1.35	1.32	1.32	1.28	1.23	1.24	1.16	1.28	1.41	1.48	1.39	1.43	1.43	1.51
Trace														
Li	135	158	149	157	171	160	170	190	194	198	160	233	194	219
P	7.06	20.2	6.55	58.2	940	53.9	13.5	17	36.4	31	24.9	26.2	29.5	24
Sc	40.9	50.2	30.5	28.4	50	60.1	69.4	18.8	23.4	53.7	52.5	25.8	36.7	20.1
V	487	603	631	316	1046	1011	1004	535	969	752	858	783	828	905
Cr	153	174	124	32.1	580	658	681	169	278	196	157	379	541	498
Co	38	47.8	43.5	38.1	38.7	37.6	34.8	44.4	50.7	48.9	52.1	48.8	55.1	47.7
Ni	33.2	52.9	35	36.6	121	121	118	55.6	58.1	66.4	40	98.9	75.1	87
Cu	0.097	1.26	0.287	0.442	0.148	0.161	0.351	0.066	0.812	0.296	0.11	0.053	0.148	0
Zn	471	520	457	438	592	582	562	497	754	760	658	804	777	726
Ga	34.3	47.1	37.3	34.5	38.5	45.2	46.1	41.1	54.4	54.2	54.6	72.7	67.2	72.7
Y	0.0772	6.26	0.144	2.26	0.209	0.393	0.176	0.601	0.5	0.24	0.142	0.098	0.14	0.285
Zr	1.15	1.28	0.968	0.883	2.38	4.42	2.15	0.523	1.32	0	0.523	0.98	1.03	2.14

Table 6. Continued

Sample Name	SC-12	SC-12	SC-8-2	SC-7-2	SC-7-2	SC-13	SC-13
Sample Type	Biotite-rich encl.	Biotite-rich encl.	Amphibolite encl.	Composite encl.	Composite encl.	Tonalite	Tonalite
No.	49	51	41	24	25	12	14
Location in sample	Enclave	Enclave	Enclave	Enclave	Enclave	Tonalite	Tonalite
SiO_2 (wt%)	35.6	36.7	38.1	37.4	34.1	36.9	32.7
TiO_2	3.24	3.4	2.95	4.32	4.03	3.73	4.12
Al_2O_3	16.9	16.8	15.8	14.6	16.6	15.5	17.3
Cr_2O_3	0.06	0.06	0.02	0.01	0.01	0.02	0.01
FeO_T	20.8	22.7	23.8	26.7	26.4	24.1	27.6
MnO	0.28	0.3	0.39	0.31	0.29	0.21	0.27
MgO	6.16	7	6.52	5.96	7.33	7.28	5.87
CaO	3.02	0.04	0.09	0.04	0.04	0.11	0.08
Na_2O	0.23	0.04	0.03	0.1	0.09	0.07	0.07
K_2O	11.4	13	12.3	10.5	11.1	12.1	11.9
P_2O_5	2.33	0	0	0	0	0.01	0
Total	100.02	100.04	100	99.94	99.99	100.03	99.92
Rare Earth Elements							
Rb (ppm)	461	544	629	394	342	527	557
Sr	0.356	0.516	0.365	0.749	0.901	0.279	0.349
Zr	0.438	0.433	0.27	2.23	0.69	0.391	0.498
Nb	39	52.8	56.3	81.4	72.3	45.2	47.1
Ba	1379	4092	1283	6689	5648	783	796
La	0.0272	0.0508	0.0519	0.0925	0.0688	0.0107	0.0114
Ce	0.047	0.044	0.118	0.09	0.0272	0.0129	0.0132
Nd	0.0757	0.0531	0.0831	0.0581	0.0434	0.0907	na
Sm	0.0317	0.0404	0.000808	0.0377	0.0196	na	0.0305
Gd	0.0201	0.028	0.0352	0.0299	0.0259	na	0.0396
Tb	0.00643	0.00492	0.000115	0.011	na	0.00879	0.00719
Dy	0.000443	0.0262	0.0313	0.0556	0.0278	0.0299	0.0316
Ho	0.00268	0.00583	0.00951	0.0161	0.00717	0.00836	0.00891
Er	0.000369	0.0273	0.0285	0.0548	0.0189	0.0151	0.0246
Yb	0.000463	0.0455	0.0303	0.0377	0.0293	0.0626	na
Lu	0.00564	0.00811	0.0136	0.0129	0.00731	na	0.00865
Hf	0.363	0.598	0.443	0.422	0.371	0.208	0.216
Ta	2.92	4.32	3.86	6.48	5.3	4.07	3.97
Th	0.114	0.0199	0.0289	0.0214	0.0737	0.0112	0.0237
U	0.0533	0.00955	0.0272	0.0614	0.0171	0.0121	0.0186

Table 7.

Sample Name	SC-8-2	SC-7-2	SC-8-2	SC-8-2
Sample Type	Amphibolite enclave	Composite enclave	Tonalite	Tonalite
No.	31	43	14	18
Location in Sample	Enclave	Enclave	Tonalite	Tonalite
SiO_2 (wt%)	53.1	53.2	55	54.9
TiO_2	1.32	0.2	0.1	0.13
Al_2O_3	9.11	2.02	1.42	1.28
Cr_2O_3	0.01	0.03	0.03	0.01
FeO_T	14.2	18.7	19.5	18.7
MnO	0.27	0.68	0.73	0.65
MgO	7.47	10.7	10.8	11.1
CaO	12.2	14	12	12.7
Na_2O	1.74	0.22	0.19	0.14
K_2O	0.48	0.15	0.11	0.07
P_2O_5	0.01	0.01	0	0.35
Total	99.91	99.91	99.88	100.03
Rare Earth Elements				
Rb (ppm)	1.22	0.149	0.582	3.3
Sr	62.2	2.99	14.7	8.89
Zr	112	1.84	3.92	4.86
Nb	0.971	0.0604	0.32	3.03
Ba	3.73	0.26	3.92	13.3
La	1.04	0.384	0.245	0.475
Ce	3.5	3.06	1.44	2.4
Nd	7.61	6	3.53	4.99
Sm	3.89	3.11	2.14	3.2
Gd	6.51	4.36	4.66	5.97
Tb	1.06	0.756	1.02	1.3
Dy	7.35	5.7	8.69	8.36
Ho	1.39	1.1	2.26	1.94
Er	3.86	2.87	8.42	5.93
Yb	2.79	1.94	10.2	4.64
Lu	0.485	0.334	1.73	0.82
Hf	3.1	0.202	0.355	0.588
Ta	0.0518	0.0119	0.0312	0.17
Th	0.744	0.0474	0.191	0.133
U	0.437	0.0357	0.564	0.498

Table 8.

Sample Name	SC-4-3	SC-4-3	SC-4-3	SC-4-3
Enclave Type	Carbonate-bearing	Carbonate-bearing	Carbonate-bearing	Carbonate-bearing
No.	26	21	17	18
Location in sample	Tonalite	Enclave rim	Enclave rim	Enclave rim
SiO_2 (wt%)	46.6	46.5	50.5	51.4
TiO_2	1.41	0.11	0.08	0.07
Al_2O_3	5.98	4.86	3.11	1.09
Cr_2O_3	0	0.01	0.01	0.01
FeO_T	24.4	27.2	23.9	18
MnO	0.69	0.61	0.62	0.77
MgO	7.58	7.64	8.68	5.71
CaO	11.6	11.9	12.5	22.5
Na_2O	1	0.63	0.41	0.37
K_2O	0.7	0.47	0.19	0.08
P_2O_5	0.01	0.01	0.01	0.01
Total	99.97	99.94	100.01	100.01
# of ions on the				
Na	0.28	0.18	0.11	0.1
Mg	1.63	1.67	1.85	1.22
Al	1.02	0.84	0.52	0.18
Si	6.75	6.82	7.21	7.36
P	0	0	0	0
K	0.13	0.09	0.03	0.01
Ca	1.8	1.87	1.91	3.46
Ti	0.15	0.01	0.01	0.01
Cr	0	0	0	0
Mn	0.08	0.08	0.08	0.09
Fe	2.95	3.33	2.85	2.15
Trace Elements (ppm)				
Li	6.24	3.6	3.17	10.4
P	45.6	44.9	52.3	58.2
Sc	1051	150	209	100
V	572	306	317	266
Cr	22.5	57.1	80.6	78.7
Co	45.6	143	46.3	27.5
Ni	20.6	282	20.6	10.4
Cu	0.342	138	0.302	0.704
Zn	659	600	622	480
Ga	24.2	26.4	11	6.53
Zr	106	9.85	4.69	7.84

Table 9.

Temperature (C)	960	930	900	870	840	810	780	750	720
Cumulate percentage	4.15	17.81	33.02	38.90	44.16	52.71	58.36	59.11	100.00
Liquid percentage	95.85	82.19	66.98	61.10	55.84	47.29	41.64	40.89	0.00
	Cumulate compositions								
SiO_2(wt.%)	35.49	43.79	47.05	48.09	49.18	50.99	51.68	51.20	62.42
TiO_2	3.49	1.90	1.44	1.33	1.32	1.28	1.25	1.30	0.85
Al_2O_3	2.70	16.97	18.52	18.75	18.91	18.70	18.79	18.48	15.19
FeO_T	31.17	16.06	12.86	12.06	11.30	10.25	9.74	9.79	6.09
MgO	13.64	5.72	4.12	3.75	3.49	3.13	2.91	2.90	1.77
CaO	3.03	7.67	7.46	7.23	7.01	6.64	6.46	6.69	4.62
Na_2O	0.00	2.41	3.46	3.79	4.03	4.32	4.50	4.72	3.32
K_2O	0.00	0.11	0.19	0.23	0.27	0.34	0.41	0.43	1.72
	Liquid Composition								
SiO_2(wt.%)	63.59	66.44	69.16	71.54	72.91	75.26	77.23	78.37	
TiO_2	0.73	0.62	0.56	0.53	0.46	0.35	0.27	0.21	
Al_2O_3	15.73	14.80	13.78	12.82	12.26	11.30	10.60	10.46	
FeO_T	5.00	3.92	3.01	2.27	1.96	1.44	0.96	0.81	
MgO	1.26	0.92	0.68	0.52	0.42	0.26	0.18	0.17	
CaO	4.69	3.95	3.37	2.95	2.73	2.36	2.03	1.68	
Na_2O	3.46	3.51	3.34	3.01	2.75	2.20	1.66	1.29	
K_2O	1.80	2.07	2.38	2.67	2.87	3.27	3.58	3.59	
	Mineralogy								
Amphibole	0.00	0.00	0.00	0.00	0.00	0.00	0.00	14.55	11.58
Quartz	0.00	0.00	0.00	0.00	0.00	0.00	0.00	0.00	20.78
Plagioclase	0.00	53.14	63.45	65.70	66.96	68.03	68.51	69.84	48.87
K-feldspar	0.00	0.00	0.00	0.00	0.00	0.00	0.00	0.00	10.72
Diopside	69.72	30.51	23.57	22.23	22.34	23.93	24.10	4.81	0.64
Spinel	20.66	11.43	8.64	7.79	5.65	1.68	0.00	5.61	2.59
Water	9.62	4.87	4.37	4.31	4.26	4.21	4.21	4.81	3.66
Ilmenite	0.00	0.00	0.00	0.00	0.82	2.14	2.55	1.25	1.17

Table 10.

Temperature (in C)	1200	1190	1180	1170	1160	1150	1140	1130	1120	1110	1100	1090	1080	1070
Solid	3.45	4.30	5.12	5.90	6.65	7.37	8.08	8.74	9.38	10.00	10.60	11.18	11.74	22.86
Liquid	96.55	95.70	94.88	94.10	93.35	92.63	91.92	91.26	90.62	90.00	89.40	88.82	88.26	77.14
Solid														
SiO_2(wt.%)	0.00	40.35	40.35	40.18	40.18	40.18	40.18	40.18	40.01	40.01	40.01	40.01	39.72	39.55
TiO_2	0.00	0.00	0.00	0.00	0.00	0.00	0.00	0.00	0.00	0.00	0.00	0.00	0.00	0.00
Al_2O_3	0.00	0.00	0.00	0.00	0.00	0.00	0.00	0.00	0.00	0.00	0.00	0.00	0.00	0.00
FeO_T	0.00	12.55	12.55	13.46	13.46	13.46	13.46	13.46	14.36	14.36	14.36	14.36	14.25	15.14
MgO	0.00	47.10	47.10	46.36	46.36	46.36	46.36	46.36	45.63	45.63	45.63	45.63	45.29	44.57
CaO	0.00	0.00	0.00	0.00	0.00	0.00	0.00	0.00	0.00	0.00	0.00	0.00	0.74	0.74
Na_2O	0.00	0.00	0.00	0.00	0.00	0.00	0.00	0.00	0.00	0.00	0.00	0.00	0.00	0.00
K_2O	0.00	0.00	0.00	0.00	0.00	0.00	0.00	0.00	0.00	0.00	0.00	0.00	0.00	0.00
H_2O	0.00	0.00	0.00	0.00	0.00	0.00	0.00	0.00	0.00	0.00	0.00	0.00	0.00	0.00
Liquid														
SiO_2(wt.%)	50.24	50.33	50.41	50.5	50.58	50.67	50.75	50.83	50.9	50.98	51.06	51.06	51.2	51.72
TiO_2	0.98	0.99	1	1	1.01	1.02	1.03	1.03	1.04	1.05	1.06	1.06	1.07	1.02
Al_2O_3	15.67	15.81	15.95	16.08	16.21	16.33	16.46	16.58	16.7	16.81	16.92	16.92	17.14	18.75
FeO_T	8.38	8.349	8.299	8.249	8.198	8.148	8.088	8.028	7.977	7.917	7.847	7.847	7.717	7.79
MgO	8.31	7.97	7.65	7.33	7.02	6.73	6.44	6.16	5.89	5.63	5.38	5.38	4.9	3.64
CaO	9.9	9.99	10.07	10.15	10.23	10.31	10.38	10.45	10.53	10.6	10.66	10.66	10.8	9.22
Na_2O	2.61	2.63	2.65	2.67	2.69	2.72	2.74	2.76	2.78	2.79	2.81	2.81	2.85	3.24
K_2O	0.88	0.89	0.89	0.9	0.91	0.92	0.92	0.93	0.94	0.94	0.95	0.95	0.96	1.1
H_2O	2.89	2.92	2.94	2.97	3	3.03	3.05	3.08	3.11	3.14	3.17	3.17	3.22	3.38
Mineralogy														
Clinopyroxene	0.00	0.00	0.00	0.00	0.00	0.00	0.00	0.00	0.00	0.00	0.00	0.00	0.00	0.00
Orthopyroxene	0.00	0.00	0.00	0.00	0.00	0.00	0.00	0.00	0.00	0.00	0.00	0.00	0.00	0.00
Plagioclase	0.00	0.00	0.00	0.00	0.00	0.00	0.00	0.00	0.00	0.00	0.00	0.00	0.00	0.00
Spinel	0.00	0.00	0.00	0.00	0.00	0.00	0.00	0.00	0.00	0.00	0.00	0.00	0.00	0.00
Diopside	0.00	0.00	0.00	0.00	0.00	0.00	0.00	0.00	0.00	0.00	0.00	0.00	0.00	0.00
Olivine	0.00	100.00	100.00	100.00	100.00	100.00	100.00	100.00	100.00	100.00	100.00	100.00	100.00	100.00
K-Feldspar	0.00	0.00	0.00	0.00	0.00	0.00	0.00	0.00	0.00	0.00	0.00	0.00	0.00	0.00

Table 10. Continued

Temperature (in C)	1060	1050	1040	1030	1020	1010	1000	990	980	970	960	950	940
Solid	25.61	30.56	34.77	38.69	43.34	47.90	51.74	55.56	58.92	61.81	64.37	66.65	68.71
Liquid	74.39	69.44	65.23	61.31	56.66	52.10	48.26	44.44	41.08	38.19	35.63	33.35	31.29
Solid													
SiO_2(wt.%)	39.55	44.57	45.06	45.34	45.30	44.86	44.53	44.30	44.29	44.42	44.49	44.57	44.80
TiO_2	0.00	0.80	0.79	0.77	1.01	1.04	1.14	1.18	1.23	1.26	1.27	1.27	1.28
Al_2O_3	0.00	3.45	6.28	8.20	9.51	10.79	11.98	12.85	13.47	14.00	14.44	14.70	14.94
FeO_T	15.14	10.82	9.65	8.88	8.76	9.35	9.61	10.00	10.26	10.35	10.45	10.51	10.56
MgO	44.57	27.45	23.98	21.80	20.05	18.42	17.32	16.49	15.65	15.01	14.52	14.07	13.71
CaO	0.74	12.70	13.91	14.55	14.87	14.83	14.54	14.14	13.92	13.68	13.47	13.35	13.12
Na_2O	0.00	0.08	0.22	0.33	0.40	0.52	0.63	0.73	0.86	0.95	1.03	1.15	1.23
K_2O	0.00	0.00	0.00	0.00	0.00	0.00	0.05	0.05	0.06	0.06	0.06	0.06	0.07
H_2O	0.00	0.00	0.00	0.00	0.00	0.00	0.00	0.00	0.00	0.00	0.00	0.00	0.00
Liquid													
SiO_2(wt.%)	51.89	52.32	52.73	53.28	54.43	55.71	56.92	58.05	59.15	60.2	61.19	62.15	63.07
TiO_2	1	1.01	1.02	0.99	0.84	0.74	0.66	0.59	0.52	0.47	0.42	0.38	0.34
Al_2O_3	19.2	19.14	19.04	18.94	18.82	18.49	18.14	17.82	17.51	17.19	16.87	16.55	16.23
FeO_T	7.8	8.076	8.332	8.44	7.967	7.493	7.039	6.575	6.131	5.717	5.323	4.968	4.614
MgO	3.29	3.07	2.89	2.72	2.56	2.29	2.07	1.85	1.63	1.44	1.28	1.13	1.01
CaO	8.76	8.03	7.35	6.71	6.09	5.62	5.18	4.75	4.34	3.96	3.61	3.27	2.96
Na_2O	3.35	3.52	3.68	3.84	4.05	4.25	4.43	4.62	4.79	4.94	5.06	5.15	5.23
K_2O	1.14	1.22	1.3	1.37	1.48	1.61	1.73	1.87	2.01	2.15	2.29	2.43	2.57
H_2O	3.44	3.47	3.51	3.55	3.61	3.66	3.71	3.75	3.79	3.82	3.85	3.87	3.88
Mineralogy													
Clinopyroxene	0.00	0.00	0.00	0.00	0.00	0.00	0.00	0.00	0.00	0.00	0.00	0.00	0.00
Orthopyroxene	0.00	0.00	0.00	0.00	0.00	0.00	0.00	0.00	0.00	0.00	0.00	0.00	0.00
Plagioclase	0.00	0.00	8.44	13.96	18.07	22.04	26.42	29.68	32.27	34.33	36.03	37.46	38.72
Spinel	0.00	0.00	0.00	0.00	0.47	2.25	3.35	4.09	4.62	4.97	5.22	5.40	5.54
Diopside	0.00	55.89	54.72	53.73	52.50	49.90	45.74	42.65	41.18	40.04	39.08	38.22	37.48
Olivine	100.00	44.11	36.84	32.31	28.98	25.82	24.49	23.56	21.93	20.67	19.69	18.91	18.26
K-Feldspar	0.00	0.00	0.00	0.00	0.00	0.00	0.00	0.00	0.00	0.00	0.00	0.00	0.00

Table 10. Continued

Temperature (in C)	930	920	910	900	890	880	870	860	850	840	830
Solid Percentage	70.61	72.36	73.99	75.53	76.98	78.37	79.86	81.16	82.46	84.02	85.36
Liquid Percentage	29.39	27.64	26.01	24.47	23.02	21.63	20.14	18.84	17.54	15.98	14.64
Solid composition											
SiO_2(wt.%)	44.95	45.07	45.31	45.40	45.60	45.75	46.00	46.19	46.37	46.70	46.95
TiO_2	1.28	1.26	1.26	1.26	1.25	1.22	1.22	1.21	1.19	1.18	1.17
Al_2O_3	15.21	15.42	15.54	15.70	15.78	15.92	15.94	16.05	16.15	16.19	16.23
FeO_T	10.48	10.54	10.47	10.49	10.41	10.35	10.37	10.30	10.23	10.14	10.04
MgO	13.38	13.09	12.81	12.62	12.41	12.20	12.01	11.83	11.66	11.49	11.28
CaO	13.00	12.85	12.71	12.54	12.48	12.41	12.15	12.04	11.94	11.75	11.56
Na_2O	1.31	1.39	1.52	1.60	1.68	1.76	1.84	1.92	2.00	2.08	2.18
K_2O	0.07	0.07	0.07	0.07	0.08	0.08	0.16	0.16	0.16	0.16	0.30
H_2O	0.00	0.00	0.00	0.00	0.00	0.00	0.00	0.00	0.00	0.00	0.00
Liquid composition											
SiO_2(wt.%)	63.96	64.83	65.68	66.52	67.35	68.17	69.05	69.9	70.78	71.82	72.85
TiO_2	0.3	0.27	0.24	0.22	0.2	0.18	0.17	0.16	0.15	0.14	0.13
Al_2O_3	15.9	15.56	15.22	14.88	14.52	14.16	13.78	13.38	12.94	12.39	11.84
FeO_T	4.289	3.984	3.689	3.414	3.158	2.903	2.648	2.442	2.246	2.099	1.971
MgO	0.9	0.8	0.72	0.64	0.57	0.51	0.4	0.35	0.31	0.27	0.23
CaO	2.67	2.4	2.14	1.91	1.69	1.49	1.31	1.16	1.03	0.97	0.92
Na_2O	5.28	5.3	5.3	5.28	5.24	5.17	5.07	4.94	4.78	4.62	4.48
K_2O	2.72	2.87	3.02	3.17	3.33	3.48	3.66	3.81	3.93	3.88	3.78
H_2O	3.89	3.9	3.9	3.89	3.88	3.86	3.84	3.82	3.79	3.77	3.75
Mineralogy											
Clinopyroxene	0.00	0.00	0.00	0.00	0.00	0.00	0.00	0.00	0.00	0.00	0.00
Orthopyroxene	0.00	0.00	0.00	0.00	0.00	0.00	0.00	0.23	0.32	0.41	0.49
Plagioclase	39.84	40.87	41.80	42.66	43.48	44.25	44.97	45.69	46.38	47.07	47.22
Spinel	5.64	5.71	5.77	5.80	5.83	5.84	5.84	5.80	5.79	5.76	5.71
Diopside	36.80	36.19	35.62	35.08	34.58	34.11	33.67	33.05	32.52	32.01	31.42
Olivine	17.71	17.23	16.81	16.44	16.11	15.80	15.52	15.23	14.99	14.75	14.48
K-Feldspar	0.00	0.00	0.00	0.00	0.00	0.00	0.00	0.00	0.00	0.00	0.68

Table 10. Continued

Temperature (in C)	820	810	800	790	780	770	760	750	740
Solid Percentage	86.43	87.31	88.05	88.67	89.21	89.68	90.10	90.46	90.62
Liquid Percentage	13.57	12.69	11.95	11.33	10.79	10.32	9.90	9.54	9.38
Solid composition									
SiO_2(wt.%)	47.24	47.37	47.63	47.68	47.75	47.96	47.96	47.95	48.04
TiO_2	1.15	1.14	1.14	1.13	1.12	1.10	1.10	1.09	1.09
Al_2O_3	16.25	16.33	16.34	16.38	16.42	16.40	16.40	16.45	16.48
FeO_T	9.93	9.85	9.79	9.73	9.69	9.66	9.65	9.57	9.57
MgO	11.12	10.99	10.88	10.80	10.73	10.67	10.61	10.53	10.54
CaO	11.37	11.30	11.16	11.11	11.07	10.95	10.92	10.88	10.86
Na_2O	2.28	2.31	2.33	2.41	2.42	2.44	2.45	2.47	2.48
K_2O	0.36	0.41	0.45	0.48	0.50	0.52	0.62	0.64	0.66
H_2O	0.00	0.00	0.00	0.00	0.00	0.00	0.00	0.00	0.00
Liquid composition									
SiO_2(wt.%)	73.82	74.72	75.58	76.39	77.16	77.9	78.6	79.32	79.97
TiO_2	0.13	0.12	0.12	0.11	0.11	0.11	0.1	0.09	0.08
Al_2O_3	11.32	10.84	10.39	9.96	9.54	9.15	8.77	8.32	7.97
FeO_T	1.834	1.707	1.599	1.491	1.374	1.276	1.178	1.119	1.031
MgO	0.2	0.18	0.16	0.14	0.12	0.11	0.09	0.08	0.07
CaO	0.89	0.86	0.83	0.81	0.79	0.78	0.76	0.72	0.71
Na_2O	4.33	4.2	4.06	3.93	3.8	3.68	3.57	3.54	3.43
K_2O	3.68	3.59	3.51	3.43	3.35	3.28	3.21	3.1	3.04
H_2O	3.74	3.73	3.72	3.71	3.7	3.69	3.68	3.68	3.67
Mineralogy									
Clinopyroxene (modal%)	0.00	0.00	0.00	0.00	0.00	0.00	0.00	0.16	0.15
Orthopyroxene	0.55	0.59	0.63	0.66	0.69	0.71	0.73	0.77	0.79
Plagioclase	47.18	47.17	47.17	47.18	47.18	47.19	47.20	47.23	47.25
Spinel	5.65	5.62	5.60	5.56	5.54	5.52	5.52	5.59	5.58
Diopside	30.92	30.54	30.23	29.98	29.77	29.59	29.44	28.76	28.65
Olivine	14.25	14.08	13.94	13.82	13.72	13.64	13.57	13.50	13.56
K-Feldspar	1.43	1.99	2.44	2.80	3.09	3.33	3.55	3.87	4.03